Tectono-thermal evolution of Oman's Mesozoic passive continental margin under the obducting Semail Ophiolite: a case study of Jebel Akhdar, Oman

Arne Grobe[1,2], Christoph von Hagke[1], Ralf Littke[2], István Dunkl[3], Franziska Wübbeler[1], Philippe Muchez[4], Janos L. Urai[1,5]

[1]Structural Geology, Tectonics, and Geomechanics, EMR Group, RWTH Aachen University, Germany
[2]Geology and Geochemistry of Petroleum and Coal, EMR Group, RWTH Aachen University, Germany
[3]Sedimentology & Environmental Geology, Geoscience Center Georg-August-Universität Göttingen, Germany
[4]Geodynamics and Geofluids Research Group, Department of Earth and Environmental Sciences, KU Leuven, Belgium
[5]Department of Applied Geoscience, German University of Technology in Oman GUtech, Muscat, Oman.

Correspondence to: Arne Grobe, arne.grobe@rwth-aachen.de, ORCID: 0000-0001-6471-0624

Keywords: basin modeling, passive margin, obduction, burial, Raman spectroscopy, thermochronology, thermal maturity

Abstract. We present a study of the pressure and temperature evolution in the passive continental margin under the Oman Ophiolite, using numerical basin models calibrated with thermal maturity data, fluid inclusion thermometry and low-temperature thermochronometry, and building on the results of recent work on the tectonic evolution. Because the Oman Mountains experienced only weak post-obduction overprint, they offer a unique natural laboratory for this study.

Thermal maturity data from the Adam Foothills constrain burial in the basin in front of the advancing nappes to at least 4 km. Peak temperature evolution in the carbonate platform under the ophiolite depends on the burial depth and only weakly on the temperature of the overriding nappes which have cooled during transport from the oceanic subduction zone to emplacement. Fluid-inclusion thermometry yields pressure-corrected homogenization temperatures of 225 to 266 °C for veins formed during progressive burial, 296-364 °C for veins related to peak burial and 184 to 213 °C for veins associated with late-stage strike-slip faulting. In contrast, the overlying Hawasina nappes have not been heated above 130-170 ℃, as witnessed by only partial resetting of the zircon (U-Th)/He thermochronometer.

In combination with independently determined temperatures from solid bitumen reflectance, we infer that the fluid inclusions of peak-burial-related veins formed at minimum pressures of 225-285 MPa. This implies that the rocks of the future Jebel Akhdar Dome were buried under 8-10 km of ophiolite on top of 2 km of sedimentary nappes, in agreement with thermal maturity data of solid bitumen reflectance and Raman spectroscopy.

Rapid burial of the passive margin under the ophiolite results in sub-lithostatic pore pressures, as indicated by veins formed in dilatant fractures in the carbonates. We infer that overpressure is induced by rapid burial under the ophiolite. Tilting of the carbonate platform in combination with overpressure in the passive margin caused fluid migration towards the south in front of the advancing nappes.

Exhumation of the Jebel Akhdar as indicated by our zircon (U-Th)/He data and in agreement with existing work on the tectonic evolution, started as early as the late Cretaceous to early Cenozoic, linked with extension above a major listric shear zone with top-to-NNE shear sense. In a second exhumation phase the carbonate platform and

40   obducted nappes of the Jebel Akhdar Dome cooled together below c. 170 °C between 50 and 40 Ma, before the

41   final stage of anticline formation.

42   **1.   Introduction**

43   The Permian-Mesozoic platform sediments of north Oman (Figure 1; e.g. Beurrier et al., 1986; Glennie et al.,

44   1974; Lippard et al., 1982) with hydrocarbon accumulations in the southern foreland of the Jebel Akhdar Dome

45   (Figures 1 and 2) are overlain by the Semail ophiolite nappe complex, the largest and best-preserved ophiolite on

46   Earth. Limited tectonic extension after obduction followed by uplift, folding and deep erosion and the present-day

47   arid climate formed exceptional exposures in three tectonic windows and in the foreland fold-and-thrust belt of

48   the Oman Mountains (Figure 1). The structural and tectonic evolution of the Oman Mountains has been one main

49   focus of our group in the last 15 years (e.g. Arndt et al., 2014; Gomez-Rivas et al., 2014; Grobe et al., 2016, 2018;

50   Hilgers et al., 2006; Holland et al., 2009a; Virgo et al., 2013a, 2013b) and was investigated in many other studies

51   focusing on tectonic history (Breton et al., 2004; Cooper et al., 2014; Glennie et al., 1973, 1974; Grobe et al., 2018;

52   Loosveld et al., 1996; Searle, 2007), stratigraphic sequences (Van Buchem et al., 2002; Grelaud et al., 2006;

53   Homewood et al., 2008), geodynamic modelling (Duretz et al., 2015), hydrocarbon source rocks (Van Buchem et

54   al., 1996; Philip et al., 1995; Scott, 1990) and reservoir rocks (Arndt et al., 2014; De Keijzer et al., 2007; Koehrer

55   et al., 2011; Virgo et al., 2013a). Less well known is the temperature and pressure evolution of the subophiolite

56   passive margin units and the subsequent cooling history of the Jebel Akhdar (Aldega et al., 2017; Grobe et al.,

57   2018; Hansman et al., 2017; Poupeau et al., 1998; Saddiqi et al., 2006). This information is vital for our

58   understanding of the time-temperature history of overthrusted margins and would allow to further constrain

59   obduction dynamics and forebulge migration. Combining peak temperature evolution with cooling ages links the

60   burial history with phases of orogeny.

61
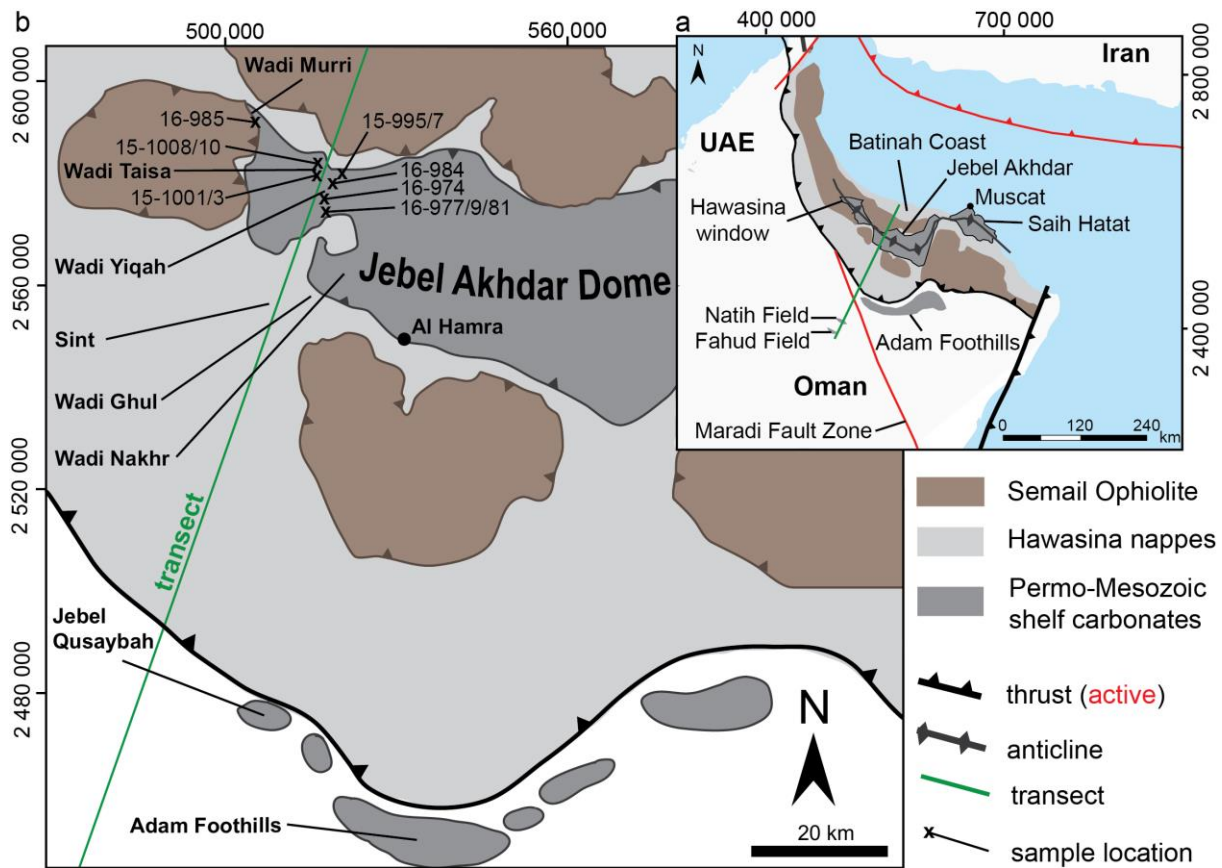
Figure 1: a) Tectonic setting of the Oman Mountains. Dark gray are the three tectonic windows of Hawasina, Jebel Akhdar and Saih Hatat as well as the Adam Foothills. Brown areas show the exposed Semail Ophiolite, black lines denote the obduction fronts of Semail and Masirah ophiolites, red lines denote lithosphere-scale, active faults. The modeled transect (black line) crosscuts the Jebel Akhdar window and continues to the Natih and Fahud oil fields in the southwestern mountain foreland. b) Geologic map of the Jebel Akhdar window with the location of the modeled transect (solid black line) and the locations of thermal maturity data (x).

In other orogens, peak temperatures related to nappe emplacement were reconstructed by analyzing thermal maturity of finely dispersed organic material (e.g. Teichmüller and Teichmüller, 1986; Zagros: Mashhadi et al., 2015; Holy Cross Mountain: Schito et al., 2017; Eastern Alps: Lünsdorf et al., 2012; Southern Alps: Rantitsch and Rainer, 2003; Apennines: Reutter et al., 1988). However, the number of studies of thermal and pressure effects on overthrust sedimentary basins is limited and modeling approaches to reconstruct such large scale overthrusts are increasing but still few (e.g. Aldega et al., 2018; Deville and Sassi, 2006; Ferreiro Mählmann, 2001; Jirman et al., 2018; Oxburgh and Turcotte, 1974; Roure et al., 2010; Schito et al., 2018; Wygrala, 1989). In these studies, a main difficulty is to differentiate between temperature history of overthrusting and overprinting by later phases of orogeny. In the Oman Mountains, peak temperatures reached by obduction have not been overprinted. The whole Permian-Mesozoic sequence of the carbonate platform below the ophiolite is well exposed, providing outcrop to study the pressure and temperature history of this rapidly buried passive-margin sequence.

In this paper we present new thermal maturity, thermochronology and fluid inclusion data, and integrate them in a numerical basin model of the pressure-temperature evolution along a transect extending from the undeformed passive margin sequence in the south to the Batinah coast in the north (Figure 2). This helps to constrain temperature and pressure conditions of maximum burial, and the time of dome formation and exhumation linked to the structural and tectonic evolution of the area (Grobe et al., 2018). Our results for the Oman Mountains can be used to understand more deformed orogens, shed light to fluid migration in the early stages of orogeny and on exhumation related to orogenic collapse.

87
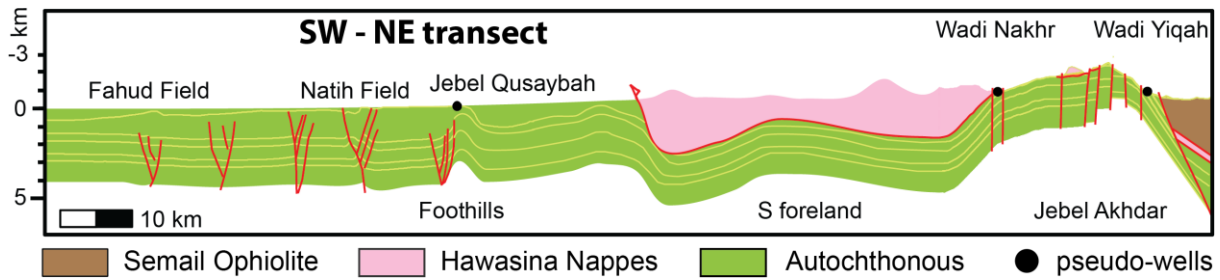
88

Figure 2: Structural transect used for modeling the Jebel Akhdar Dome and its southern foreland (Al-Lazki et al., 2002; Filbrandt et al., 2006; Searle, 2007; Warburton et al., 1990). Highlighted are the locations of the pseudo-wells (black circles) in Wadi Nakhr, Wadi Yiqah and at Jebel Qusaybah, Adam Foothills, which were used for model calibration.

2. Geological setting

2.1. Tectonic setting

Along the northeastern coast of Arabia, the NW-SE oriented Oman Mountains form a more than 400 km long anticlinal orogen (Figure 1). The mountain belt consists of allochthonous sedimentary and ophiolitic nappes thrust onto a Permian-Mesozoic passive continental margin (Breton et al., 2004; Glennie et al., 1973; Loosveld et al., 1996; Searle and Cox, 2002).

This continental margin was formed during opening of the Neotethyan ocean (Loosveld et al., 1996) and the formation of the Permian-Mesozoic Hawasina Basin (Béchennec et al., 1988; Bernoulli et al., 1990). The initiation of subsea thrusting of the future Semail Ophiolite onto the Arabian Plate at 97-92 Ma, is recorded by U-Pb geochronology (Rioux et al., 2013, 2016; Warren et al., 2005) and $^{40}Ar/^{39}Ar$ dating of the metamorphic sole (Hacker et al., 1996). The advancing ophiolite caused a flexural forebulge that moved southwestwards through the passive margin during the Upper Cretaceous (Robertson, 1987). Forebulge migration induced up to 1100 m of uplift of the Permian-Mesozoic Arabian Platform and erosion of the Cretaceous platform sediments (Searle, 2007), causing the Wasia-Aruma Break (Robertson, 1987).

During this convergence, parts of the Hawasina ocean sediments and volcanic units became detached and accreted in front of and beneath the ophiolite nappe (Béchennec et al., 1988, 1990; Glennie et al., 1974; Searle et al., 2003; Warburton et al., 1990). Palinspastic reconstructions of the Hawasina Nappes locate the position of the initial ophiolite thrusting 300-400 km offshore the Arabian coast (Béchennec et al., 1988; Glennie et al., 1974).

In the carbonate platform, burial under the advancing nappes led to generation of overpressure cells and formation of three crack-seal calcite vein generations (Gomez-Rivas et al., 2014; Grobe et al., 2018; Hilgers et al., 2006; Holland et al., 2009a; Virgo, 2015). The highest grades of metamorphism is recorded by eclogites exposed in As Sifah (Figure 1a), at c. 79 Ma (Warren et al., 2003).

The sedimentary record in the Batinah coast and the foreland, as well as laterite formation on top of the ophiolite suggest subaerial exposure and a slow-down or stopped obduction before lower marine conditions were restored in the Maastrichtian (Coleman, 1981; Forbes et al., 2010; Nolan et al., 1990). This slowdown might relate to the formation of the Makran subduction zone (Agard et al., 2005; Grobe et al., 2018; Hassanzadeh and Wernicke, 2016; Jacobs et al., 2015; Mouthereau, 2011) preserving the early stage of the obduction orogen in Oman.

In the Jebel Akhdar, post-obduction extension took place along ductile top-to-NNE shear zones, at 64 ± 4 Ma (Grobe et al., 2018; Hansman et al., 2018), followed by NW-SE striking normal fault systems (Al-Wardi and

121   Butler, 2007; Fournier et al., 2006; Grobe et al., 2018; Hanna, 1990; Hilgers et al., 2006; Holland et al., 2009a,

122   2009b; Loosveld et al., 1996; Mattern and Scharf, 2018; Virgo, 2015).

123   Renewed Arabia-Eurasia convergence during the Cenozoic formed the three dome structures. Timing of formation

124   and exhumation of the Jebel Akhdar Dome is still debated. Stratigraphic arguments for a late Cretaceous doming

125   are Maastrichtian rocks unconformably deposited on Hawasina (Bernoulli et al., 1990; Fournier et al., 2006;

126   Hanna, 1990; Nolan et al., 1990), while inclined Miocene strata at the northern fringes of the dome points to a

127   Miocene doming (Glennie et al., 1973). Consequently, some models suggest a two-phased exhumation in

128   Cretaceous and Miocene (Grobe et al., 2018; Searle, 1985, 2007), in agreement with thermochronological

129   constraints and an interpreted two-stage cooling with possible reheating in late Miocene (Poupeau et al., 1998;

130   Saddiqi et al., 2006). More recent studies, however, have shown that the data can also be explained by a cooling-

131   only scenario with exhumation in the Eocene (Hansman et al., 2017). This is in agreement with recent structural

132   observations suggesting early dome formation and later amplification of the structure (Grobe et al., 2018).

133   **2.2.**   **Stratigraphic sequence**

134   Sediments in the Jebel Akhdar area consist of a pre-Permian sequence (Autochthonous A, Figure 3) unconformably

135   overlain by a Permian-Mesozoic sequence (Autochthonous B, Figure 3; Beurrier et al., 1986; Breton et al., 2004;

136   Glennie et al., 1974; Rabu et al., 1990). During the late Cretaceous, Hawasina nappes and the Semail Ophiolite

137   were emplaced onto the passive margin, and neo-autochthonous rocks of Cenozoic age were deposited on top of

138   the ophiolite after obduction (Béchennec et al., 1988; Forbes et al., 2010; Loosveld et al., 1996).
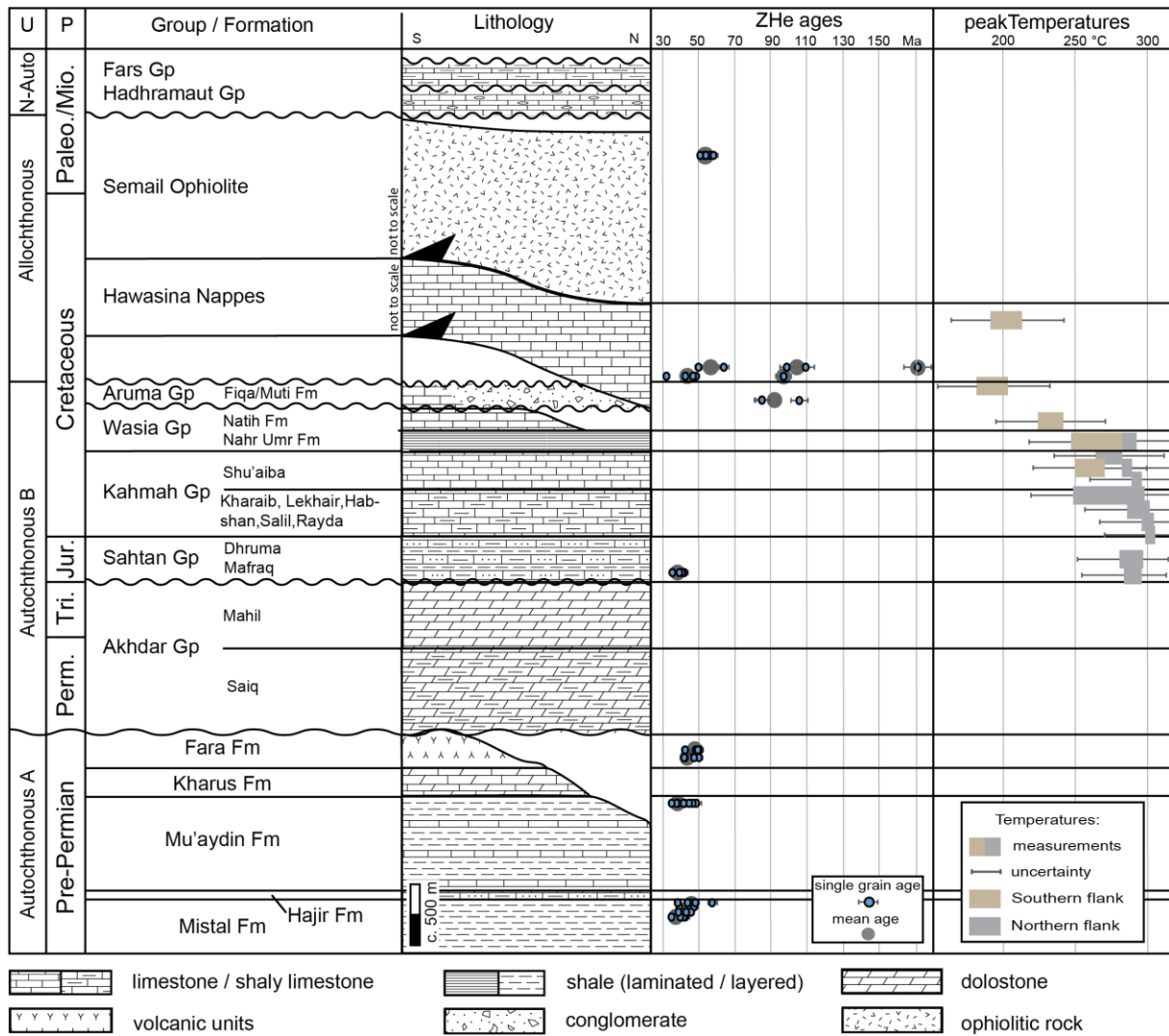
139

140 **Figure 3: Stratigraphy of the Jebel Akhdar area with its two passive margin sequences Autochthonous A and B**
141 **overthrust by Hawasina and Semail Nappes and unconformably overlain by neo-autochthonous units. Thermal**
142 **calibration data is shown: ZHe ages (Table 2) show two different grain age clusters. Peak burial temperatures from**
143 **organic matter maturity (Table 1) outline the temperature increase with stratigraphic age. Temperatures shown relate**
144 **to the measurements and related uncertainties of the calculations (U = Unit, P =Period). Note that the Semail and**
145 **Hawasina nappes are shown in their structural rather than stratigraphic positions; lithological data is compiled from**
146 **Beurrier et al. (1986), Loosveld et al. (1996), Terken et al. (2001) and Forbes et al. (2010).**

147 Autochthonous A deposits are exposed in the Jebel Akhdar window down to the Mistal Fm. (Beurrier et al., 1986).

148 Black limestones of the Hajir Fm., mudstone rich carbonate beds of the Mu'aydin Fm. and lime- and dolostones

149 of the Kharus Fm. conformably overlie the Mistal Fm. (Beurrier et al., 1986; Glennie et al., 1974). Platform break-

150 up is recorded by laminated cherts and volcanoclastics of the Fara Fm. (Beurrier et al., 1986) followed by an

151 unconformity representing a gap from Cambrian to Permian times (Loosveld et al., 1996). After establishment of

152 the Neotethyan Ocean during the Permian, northern Oman returned to stable passive margin conditions and the

153 carbonate platform of the Autochthonous B developed, with the Akhdar Group at its base (Koehrer et al., 2010;

154 Pöppelreiter et al., 2011). This is unconformably overlain by limestones with clastic interlayers of the Jurassic

155 Sahtan Group (Beurrier et al., 1986; Pratt et al., 1990). Limestones with marly, frequently organic-rich

156 intercalations of the Cretaceous Kahmah (Habsi et al., 2014; Vahrenkamp, 2010) and Wasia groups (Grelaud et

157 al., 2006; Homewood et al., 2008; Philip et al., 1995) form the youngest platform sediments (Robertson, 1987;

158 Warburton et al., 1990).

159 The obduction-related moving forebulge and associated uplift ended passive margin deposition and eroded the
160 topmost Wasia Group (Natih Fm.) in the Jebel Akdhar (Figure 3), and deeper in the Saih Hatat region. Deposition
161 in the foredeep basins in front and behind the forebulge was dominated by the syn- and postorogenic,
162 conglomerate-rich sediments of the Muti Fm., Aruma Group (Beurrier et al., 1986; Robertson, 1987). Towards the
163 south, in the Adam Foothills, this laterally grades to calcareous foreland sediments of the Fiqa Fm. (Forbes et al.,
164 2010; Robertson, 1987; Warburton et al., 1990).

165 Hawasina sediments accreted in front and beneath the ophiolite represent marine slope and basin facies, time
166 equivalent to the Autochthonous B (Béchennec et al., 1990). They are defined as four age-equivalent groups
167 (Hamrat Duru, Al Aridh, Kawr and Umar) representing carbonatic turbidite deposits (Hamrat Duru Group),
168 radiolarian cherts and platform carbonates (Al Aridh Group), platform carbonates (Kawr Group) and interbedded
169 carbonates and volcanics (Umar Group, Béchennec et al., 1990). After obduction of oceanic crust onto the passive
170 margin, neo-autochthonous evaporites and carbonates of the Paleocene to Eocene Hadhramaut Gp. and bivalve-
171 rich dolomites and limestones of the Oligo- to Pliocene Fars Group were deposited south of the mountains
172 (Béchennec et al., 1990; Forbes et al., 2010). Paleogeographic reconstructions show that the Oman Mountains had
173 high relief after obduction, followed by a low relief landscape until the early Eocene (Nolan et al., 1990). In the
174 middle Eocene marine transgression caused widespread deposition of limestones, as witnessed e.g. by the Seeb
175 and Ruwaydah Formations (Nolan et al., 1990). Post Eocene times show renewed relief development and
176 continued uplift until recent times (Glennie et al., 1974; Searle, 2007).

2.3.   Previous paleothermal data of the Autochthon

178 Only limited paleo-temperature data are available from the carbonate platform (Fink et al., 2015; Grobe et al.,
179 2016; Holland et al., 2009a; Stenhouse, 2014). Peak-burial temperatures of 226-239 °C for the top of the platform
180 were measured using solid bitumen reflectance (also referred to as pyrobitumen reflectance) and Raman
181 spectroscopy of carbonaceous material (RSCM) in the Jebel Akhdar (Grobe et al., 2016). Results indicate peak-
182 burial temperatures of 266 to 300 °C (Grobe et al., 2016; Table 1). Temperature estimates based on RSCM and
183 solid bitumen reflectance (Grobe et al., 2016) yielded similar temperatures for the southern flank of 248-280 °C
184 for the Nahr Umr, 226-239 °C for the Natih B and 172-206 °C for the Muti, respectively (Table 1, Figure 3).

185 Vein crystallization temperatures of 166-205 °C at the top of the Natih A (near Al Hamra) were measured by
186 quartz-calcite thermometry in veins formed during ophiolite-induced burial (Gen. III of Grobe et al., 2018), and
187 approximately 255 °C for veins associated with a later normal fault network (Gen V of Grobe et al., 2018;
188 Stenhouse, 2014). Fluid inclusions (FI) of bedding parallel pinch-and-swell veins (top-to-NNE shear after peak
189 burial, Gen. IV of Grobe et al., 2018) show uncorrected minimum trapping temperatures of 134-221 °C in the
190 lower beds of the Sahtan Group at Wadi Nakhr (Holland et al., 2009a). Reflectance measurements of solid-
191 bitumen-containing veins in the Wadi Ghul (Gen I of Grobe et al., 2018), which are interpreted to be associated
192 with fluid mobilization during forebulge migration, show maximum temperatures of 230 °C (Fink et al., 2015).
193 Vitrinite reflectance data of Mozafari et al. (2015) shows temperatures of c. 140 °C for the Natih B in the Jebel
194 Qusaybah, Adam Foothills, an area not overthrust by the ophiolite complex.

2.4.   Temperature evolution of the Semail Ophiolite nappe / Allochthon

196 Initial intra-oceanic ophiolite thrusting and associated metamorphism at its sole took place at peak temperatures
197 of 840 ± 70 °C at 97-92 Ma measured at several locations in the Oman Mountains (Gnos and Peters, 1993; Hacker

198   and Mosenfelder, 1996; Rioux et al., 2013; Searle and Cox, 2002; Warren et al., 2003). At 90-85 Ma the base of
199   the ophiolite cooled to 350 ± 50 °C (white mica Ar/Ar dating, Gnos and Peters, 1993). At around 80 Ma the deepest
200   burial of the Oman margin beneath the ophiolite was reached (Hacker and Mosenfelder, 1996; Warren et al., 2005)
201   with temperatures in the metamorphic sole below 300 °C (Le Metour et al., 1990; Saddiqi et al., 2006). A
202   lithospheric scale thermo-mechanical model of the thrusting in northwestern Oman includes a thermal anomaly
203   c. 100 km northwest offshore the Arabian margin to initiate subsea thrusting (Duretz et al., 2015).

2.5.   Petroleum system elements

205   Several petroleum systems developed in the carbonate platform of northern Oman with important source rock
206   horizons in the Natih Fm. (Members B and E). Both members contain Type I/II kerogen with total organic carbon
207   contents up to 15 % in the Natih B and up to 5 % in the Natih E, respectively (Terken, 1999). Source rock maturity
208   is restored based on biomarker analysis to c. 0.7 % VR within the Fahud reservoir and c. 0.9 % VR in the Natih
209   reservoir (Terken, 1999). In the southern mountain foreland Natih oil generation started in the middle Cretaceous
210   and continuous until present (Terken, 1999). Ophiolite obduction in the Jebel Akhdar area of northern Oman led
211   to over-mature Natih source rocks (Grobe et al., 2016). The Natih is classified as supercharged, laterally drained,
212   foreland petroleum system (Terken et al., 2001). However, the thermal impact of the moving forebulge and the
213   importance of tectonic processes for fluid migration below and in front of the obduction orogen are not clear. At
214   least three different generations of solid bitumen particles in veins and source rocks on the southern slope of the
215   Jebel Akhdar suggest pulses of hydrocarbon generation and migration in front of the Oman Mountains (Fink et al.,
216   2015; Grobe et al., 2016). In central Oman, Shu'aiba and Tuwaiq oils are produced out of Kahmah and Sahtan
217   Group reservoirs, sealed by argillaceous shales of the Nahr Umr Fm. (Terken et al., 2001). All these units are well-
218   exposed in the Oman Mountains.

3.   Methods

3.1.   Raman spectroscopy of carbonaceous material

221   To determine levels of thermal maturity, over 100 dark, unweathered and organic-rich samples were taken from
222   different stratigraphic units in the Jebel Akhdar (Sahtan Group, Kharaib Fm., Shu'aiba Fm., Nahr Umr Fm., Natih
223   Fm., Muti Fm., Figure 3). Based on total organic carbon (TOC) content as determined by Grobe et al. (2016), 13
224   samples were selected for thermal maturity analysis on surfaces cut perpendicular to bedding. Results were used
225   to calibrate peak-burial temperatures of the numerical basin models. The organic particles lack sufficient size or
226   surface quality for reflectance measurements and are therefore investigated by confocal Raman spectroscopy of
227   carbonaceous material. The technique measures vibrational energies of chemical bonds which change during
228   temperature induced reorganization of amorphous carbonaceous material (kerogen) to graphite (e.g. Aoya et al.,
229   2010; Beyssac et al., 2002; Kouketsu et al., 2014; Mair et al., 2018). Measurements were conducted at the
230   Geoscience Center, Göttingen, on a Horiba Jobin Yvon HR800 UV spectrometer attached to an Olympus BX-41
231   microscope and a 100× objective. A high-power diode laser with a wavelength of 488 nm and an output power of
232   50 mW was installed and a D1 filter avoided sample alteration by heating. Each spectral window (center at
233   1399.82 cm^{-1}, grid of 600 lines/mm) was measured 5 to 10 times for 2 to 10 seconds with a Peltier CCD detector
234   at activated intensity correction. For quality control, the 520.4 cm^{-1} line of a Si-wafer was measured every 30

235 minutes without observable drift of the measurements. To transform the measured data into VR_r values the scaled

236 total area (STA) approach of Lünsdorf (2016) was applied with the equation of Grobe et al. (2016):

237
$$VR_r = -\frac{STA - 280.13}{24.71} \quad [\%]$$

238 Absolute errors of the applied calibration are in the order of $\pm$ 40 °C, based on comparing neighboring samples

239 (Grobe et al., 2016) we can resolve the relative differences down to $\pm$ 30 °C which also represents the residual

240 error interpreted to relate to within-sample heterogeneity (Lünsdorf et al., 2017; Nibourel et al., 2018).

241 **3.2.   Fluid inclusion thermometry**

242 Doubly-polished wafers (c. 200 µm thick) of four vein samples (FI-N1, -N2, -M1, -M2) have been prepared

243 according to the procedure described by Muchez et al. (1994). Fluid inclusion (FI) petrography and

244 microthermometry was performed to analyze the temperature-pressure conditions and fluid's salinity. FIs represent

245 paleofluids accidentally trapped in a crystalline or amorphous solid during crystallization, lithification or both

246 (Diamond, 2003). If unaffected by later changes, trapping pressure and temperature is given by the homogenization

247 temperature (Barker and Goldstein, 1990). Based on the time of trapping primary (mineral growth), secondary

248 (fracture-related) and pseudosecondary inclusions are distinguished (Barker and Goldstein, 1990; Diamond, 2003;

249 Goldstein, 2001; Van Den Kerkhof and Hein, 2001):

250 Two calcite vein samples of the Natih Fm. (FI-N1 and 2, Locations Figure 4) represent conditions related to early

251 burial (FI-N2, structural generation I of Grobe et al., 2018), and burial beneath the ophiolite (FI-N1, structural

252 generation III of Grobe et al., 2018). Two quartz-rich calcite veins of the Muti Fm. (FI-M1 and 2, Locations Figure

253 4) are related to late, NE-SW striking strike slip faults (generation IX of Grobe et al., 2018). FI assemblages were

254 defined and fluid inclusions measured with a Linkam THMSG600 thermostage (accuracy $\pm$ 0.1 °C) attached to an

255 Olympus BX60 microscope at the KU Leuven, Belgium. Calibration was performed using CO_2, H_2O-NaCl, H_2O-

256 KCl, and H_2O standards. Homogenization temperatures (T_h) were measured prior to temperatures of complete

257 freezing (T_f), first melt (T_{fm}), and complete melting of ice ($T_{m(ice)}$) to avoid stretching or leakage due to the volume

258 increase during ice formation. All measured temperatures were recorded during heating, except for the freezing

259 temperature (T_f). Pressure corrections of T_h were conducted with the program FLINCOR (Brown, 1989) for

260 280 and 340 MPa, assuming 8 to 10 km of ophiolite overburden (see model results, ρ= c. 3070 kg/m³) and 2 km

261 of Hawasina Nappes (ρ= c. 2450 kg/m³), and for 45 MPa, assuming 2 km of sedimentary overburden (Al-Lazki et

262 al., 2002; Grobe et al., 2016). Fluid salinities were calculated from the $T_{m(ice)}$ values considering a H_2O-NaCl

263 composition (Bodnar, 1993), which is based on the T_{fm} values.

264 **3.3.   Thermochronometry**

265 Zircon (U-Th)/He (ZHe) dating allows to reconstruct the thermal history of the topmost few kilometers of the

266 Earth's crust. Helium retention in less metamict zircon crystals is sensitive in the temperature range between c. 130

267 and 170 °C, i.e. the zircon partial retention zone (PRZ, Reiners, 2005). 11 rocks sampled above (Muti Fm., Matbat

268 Fm. of the Hamrat Duru Group and Trondjemite of the Semail nappes), below (Mistal Fm., Muaydin Fm., Fara

269 Fm.) and within (Sahtan Gp.) the carbonate platform were selected for ZHe dating. Zircon crystals were released

270 using high voltage pulse crushing (http://www.selfrag.com) and concentrated by standard mineral separation

271 processes (drying, dry sieving, magnetic and heavy liquid separation). Three to eight clear, intact, euhedral single

272 crystals were selected per sample and transferred into platinum micro-capsules. They were degassed under high

vacuum by heating with an infrared diode and extracted gas purified using a SAES Ti-Zr getter at 450 °C. Helium was analyzed with a Hiden triple-filter quadrupole mass spectrometer. Degassed zircons were subsequently dissolved in pressurized teflon bombs, spiked and U, Th and Sm measured with a Perkin Elmer Elan DRC II ICP-MS equipped with an APEX micro flow nebulizer.

Time-temperature histories were reconstructed using the HeFTy 1.8.3 software package (Ketcham, 2005) applying kinetic zircon properties of Guenther et al. (2013). For samples with reset zircons the only constraint used was a minimum temperature above 200 °C between deposition and the calculated ZHe age. Thermal modeling was conducted until 100 statistically good time-temperature paths were achieved (goodness of fit: 0.5, value for acceptable fit: 0.05). In cases where this was not possible, at least 10,000 independent paths were calculated.

3.4.   Numerical basin modeling

Structural evolution was palinspastically reconstructed starting from the present-day profile using Move 2D (2016.1, Midland Valley Exploration). Geometries and relative ages of the structures were supplemented with subsurface data (Al-Lazki et al., 2002; Filbrandt et al., 2006; Searle et al., 2004; Warburton et al., 1990). The reconstruction workflow is based on restoring the pre-deformation layer continuity as follows: (1) faulted layers in the southern foreland were restored, (2) doming was retro-deformed by vertical simple shear, before (3) normal faults in the Jebel Akhdar were restored. This sequence is based on our tectonic model (Grobe et al., 2018). The resulting geometries were used as pre-thrusting input geometries for 2D PetroMod 2014.1 (Schlumberger) basin modeling, enabling thermal maturity reconstruction for vitrinite reflectance values of 0.3 to 4.7 % by the use of the EASY % Ro approach (Sweeney and Burnham, 1990). The numerical basin model is based on a conceptional definition of events. Based on this sequence of events (sedimentation, erosion, hiatus) a forward, event-stepping modeling was performed, starting with the deposition of the oldest layer. Subsequent deposition and burial is leading to differential compaction of the single rock units. For each event lithologies and related petrophysical rock properties were assigned (Figures S1, S2).

For our conceptual model the following sequence of events was implemented (Figure 3): (1) passive margin carbonate sedimentation from Permian until late Cenomanian times (Forbes et al., 2010; Loosveld et al., 1996), interrupted by a short erosional period at the Triassic-Jurassic boundary (Koehrer et al., 2010; Loosveld et al., 1996), (2) a moving forebulge associated with a paleo-water depth increase in its foredeep and erosion of the top of the carbonate platform in the north of the transect (Robertson, 1987), (3) the emplacement of allochthonous sedimentary nappes and (4) subsequent, stepwise obduction of the ophiolite with deepest burial reached at c. 79 Ma (Warren et al., 2005). Modelling ophiolite obduction as rapid emplacement accounts for burial related heat effects in the carbonate platform underneath but does not allow to fully restore the temperatures within the ophiolitic or sedimentary nappes. The area of the Adam Foothills, represented in the transect by Jebel Qusaybah, is a relic of the moving forebulge not overthrust by allochthonous units – this was used to calibrate burial depth of the foredeep at this point in the transect. The area to the south of the Adam foothills is unaffected by foredeep sedimentation, but also lacks thermal calibration data. Absolute ages, thicknesses, lithologies and related petrophysical properties as well as source rock properties were associated according to results of our own field mapping and the compiled data from Forbes et al. (2010; Figure S1).

Thermal boundary conditions of the model have been defined for each time step by the basal heat flow (HF) and the sediment water interface temperature (SWIT), representing the upper thermal boundary (Figure S3). To account for active margin tectonics and uplift and exhumation of the Jebel Akhdar, we assume an increase in basal

heat flow since the late Cretaceous. The resulting heat flow trend (Figure S3, Terken et al., 2001; Visser, 1991) has been assigned to the entire transect and was tested in the sensitivity analysis. Paleo-surface temperatures were estimated based on Oman's paleo-latitude (after Wygrala, 1989) corrected by the effect of the paleo-water depth (PWD) derived from the facies record (Van Buchem et al., 2002; Immenhauser et al., 1999; Immenhauser and Scott, 2002; Koehrer et al., 2010; Pratt et al., 1990; Robertson, 1987). This assumes that a possible heat source from the ophiolite itself does not significantly affect the temperature evolution of the top of the carbonate platform (see discussion).

This set-up has been iterated until modeling results fit the thermal calibration data (Table 1). From VR_r calculations peak-burial temperatures were determined following the approach of Barker and Pawlewicz (1994). For calibration of the numerical basin models, data was supplemented by thermal maturity and peak-burial temperature data of 63 Natih B source rock samples, taken around the Jebel Akhdar Dome (Grobe et al., 2016), and data from the Adam Foothills on Jebel Qusaybah (Mozafari et al., 2015).

Main modelling uncertainties derive from the uncertainty in thickness of paleo-overburden (Muti Fm., Ophiolite, Hawasina Nappes) and uncertainty of paleo-basal heat flow. Present-day heat flow was calibrated by data and borehole temperatures of Visser (1991) and Rolandone et al. (2013) and peak-burial temperatures determined by Raman spectroscopy and solid bitumen reflectance data (Table 1). From surface samples and their position in the stratigraphic column various pseudo-wells were created (e.g. Nöth et al., 2001) and used as control points for the 2D model (Figure 2). The model was used for sensitivity analyses of different input parameters.

4. Results and Interpretation

4.1. Thermal maturity and host rock burial temperatures

New Raman spectroscopy data of the northern flank are shown in Table 1 and give scaled total areas of 78-172. This correspond to peak temperatures of 270-300 °C in the Shu'aiba Fm., 268-305 °C in the Kahmah Group, 283-286 °C in the Sahtan Group, 270-288 °C in the Nahr Umr Fm. and c. 266 °C at the base of the Natih Fm. Based on the calculation to VR_r and temperature an absolute error of ± 30 °C has to be considered for the single values. Thermal maturity data of the Natih Fm. show solid bitumen reflectances of 2.95-3.72 % for the southern flank of the Jebel Akhdar (Fink et al, 2015, Grobe et al., 2016), 3.32 % BR for the northern flank (Grobe et al., 2016) and a single measurement of 1.1 % VR exists for the Jebel Qusaybah (Mozafari et al., 2015).

Calculated peak temperatures for the autochthonous Cretaceous deposits in the Jebel Akhdar range between 225 and 305 °C (± 30 °C, error of the calibration), two Jurassic samples 283 and 286 °C (± 30 °C). Temperatures are generally higher on the northern flank (grey boxes, Figure 3) of the Jebel Akhdar and slightly increase with stratigraphy in the autochthonous. Samples of the Muti Fm. (178-208 ± 30 °C) and the Hawasina nappes (193-213± 30 °C) show lower temperatures compared to the autochthonous. A single sample from the Jebel Qusaybah reflects peak temperatures of c. 140 °C (Table 1) in an area that was not overthrusted by nappes but buried in the related moving forebulge.

Table 1: Thermal maturity data and calculated peak temperatures of northern Oman (new data highlighted by bold sample name). Temperatures from Raman spectroscopy of carbonaceous material are calculated based on the STA approach of Lünsdorf (2016) and the equation of Grobe et. al (2016). M/P indicate if measurement was conducted on solid bitumen particles (P) or organic rich matrix (M). Errors shown relate to the measurements, calculation errors are in the order of +/-30 °C. Data in brackets is interpreted to be too low (Nahr Umr) or too high (Natih Vein, Fink et al. 2015).

sample No.		location (UTM 40Q)				No. of measurements	mean D_STA	calculated VR_r [%]	temperature range
15_995		Wadi Yiqah	516683	2582911	Sahtan Gp.	M	14	113 +/- 14	6,52	286 +/- 6 °C
15_997		Wadi Yiqah	517815	2583645	Shu'aiba Fm.	M	10	115 +/- 5	6,69	289 +/- 3 °C
15_1001		Wadi Taisa	516538	2584640	Kahmah Gp.	M	1	78	8,19	305 °C
15_1003		Wadi Taisa	516538	2584640	Kahmah Gp.	M	8	96 +/- 9	7,44	297 +/- 4 °C
15_1008	northern flank	Wadi Taisa	516562	2584727	Kahmah Gp. (top)	M	8	113 +/- 15	6,78	290 +/- 7 °C
15_1010		Wadi Taisa	516693	2584882	Shu'aiba Fm.	M	13	98 +/- 11	7,28	295 +/- 5 °C
15_1010		Wadi Taisa	516693	2584882	Shu'aiba Fm.	P	4	149 +/- 15	5,31	270 +/- 9 °C
16_974		Tr- Jur fault	515839	2582229	base Sahtan Gp.	P	6	125 +/- 17	6,29	283 +/- 9 °C
16_977		Kharb Plateau	520420	2577490	base Natih Fm.	M	10	156 +/- 9	5,04	266 +/- 6 °C
16_979		Kharb Plateau	519305	2577363	top Nahr Umr Fm.	M	2	117 +/- 4	6,60	288 +/- 2 °C
16_981		Kharb Plateau	519933	2577201	top Nahr Umr Fm.	M	1	149	5,30	270 °C
16_984		Wadi Taisa	518069	2583462	Kahmah Gp.	M	3	172 +/- 26	5,29	268 +/- 22 °C
16_985		Wadi Murri	505508	2592709	Shu'aiba Fm.	M	2	90 +/- 4	7,69	300 +/- 2 °C
Grobe et al. (2016)_SV10		Wadi Nakhr	521260	2560364	Natih	P	6	-	2,83	227-231 °C
Grobe et al. (2016)_AG22		Wadi Nakhr	521255	2560362	Natih	M	4	-	3,72	225-260 °C
Grobe et al. (2016)_AG01		Wadi Nakhr	520375	2562026	Shu'aiba (Kh 3)	M	4	-	4,49	251-269 °C
Grobe et al. (2016)_AG11		Sint	505627	2564136	Hawasina	P	5	-	2,45	193-213 °C
Grobe et al. (2016)_AG25	southern flank	Balcony Walk Nakhr	520913	2565658	Nahr Umr	M	4	-	4,23	226-267 °C
Grobe et al. (2016)_AG26_1		Balcony Walk Nakhr	521052	2565560	Nahr Umr	P	2	-	(2.58)	(211-213 °C)
Grobe et al. (2016)_AG26_3		Balcony Walk Nakhr	521052	2565560	Nahr Umr	M	2	-	4,96	275-280 °C
Grobe et al. (2016)_AG27		Balcony Walk Nakhr	520879	2565342	Nahr Umr	M	3	-	4,61	248-266 °C
Grobe et al. (2016)_AG30		Balcony Walk Nakhr	520756	2565030	Nahr Umr	M	3	-	4,25	248-257 °C
Grobe et al. (2016)_AG37		Jebel Shams	514821	2568047	Muti	P	3	-	2,16	191-208 °C
Grobe et al. (2016)_AG38		Jebel Shams	514930	2567334	Muti	P	2	-	1,99	172-206 °C

reference		location (UTM 40Q)				No. of measured particles	measured BR_r [%]	calculated / measured VR_r [%]	calculated T_burial (Barker and Pawlewicz, 1994)
Grobe et al. (2016)		Wadi Nakhr area	521216	2560308	Natih B	BR_r	253	3.08-3.59	3.08-3.59	226-239 °C
Fink et al. (2015)	south. fl.	Wadi Nakhr area	518550	2561000	Natih B	BR_r	200	3.10-3.14	3.06-3.09	225-227 °C
Fink et al. (2015)		Wadi Nakhr area	514800	2565950	Natih A Vein	BR_r	c. 250	3.40-3.76	(3.31-3.61)	(232-239 °C)
Grobe et al. (2016)		Al Hamra area	531024	2557020	Natih B	BR_r	20	2.95-3.34	2.95-3.34	223-233 °C
Grobe et al. (2016)	N	Wadi Sahtan	531010	2585640	Natih B	BR_r	6	3,32	3,32	232 °C
Mozafari et al. (2015)		Jebel Qusaybah	507930	2491600	Natih B	VR_r	20	-	1,1	c. 140 °C

353

4.2. Thermochronology

Results of the ZHe dating are shown in Figures 3 and 4; time-temperature paths modeled with HeFTy are included in the electronic supplement (Figures S4 and S5). Samples from the carbonate platform (stratigraphically older than Muti Fm.) have been entirely reset after deposition, as witnessed by Neogene apparent ages. Similarly, cooling ages from the center of the Jebel Akhdar Dome fall in the range of 48.7 ± 1.8 to 39.8 ± 3.0 Ma (Table 2, Figure 4). Sample T4, collected in the Muti Fm., yields an apparent mean age of 93.8 ± 6.9 Ma and samples T5 and T7 of the Hawasina Nappes collected at the northern and the southern slope of the dome, show two grain age clusters of $43.0 \pm 3.7 / 99.2 \pm 8.5$ Ma, and $58.9 \pm 7.0 / 106.0 \pm 5.2$ Ma, respectively. In sample T5, an additional single grain age of 172.9 ± 14.9 Ma was obtained.

364
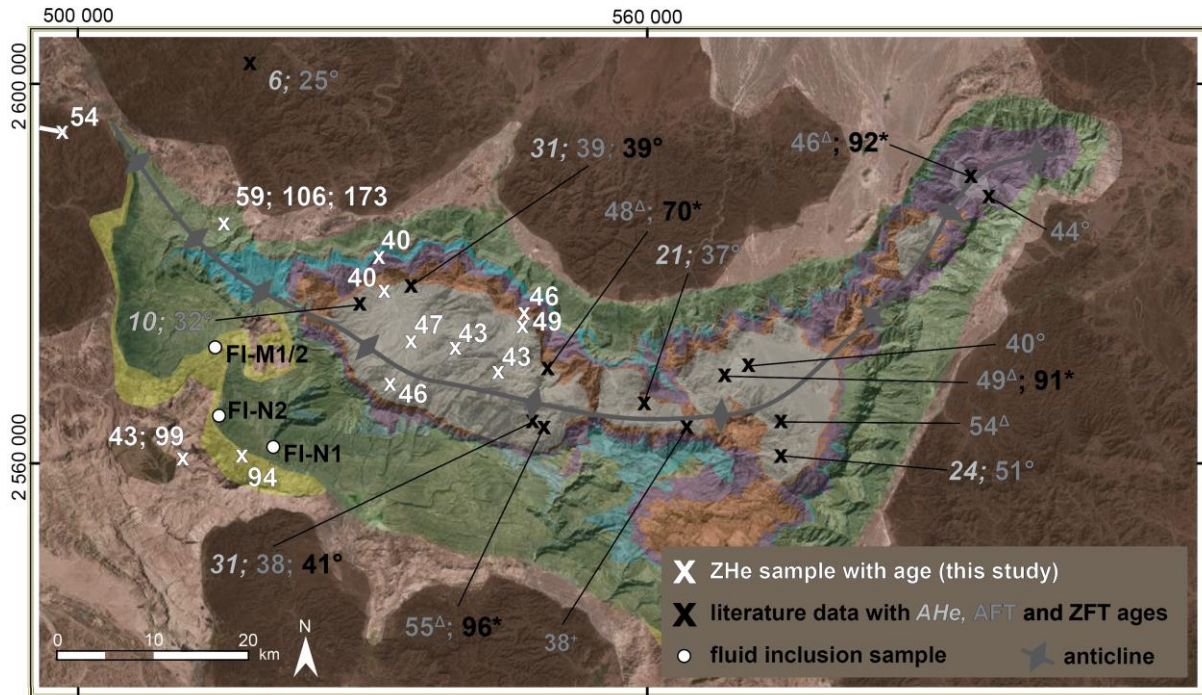
Figure 4: Map view of ZHe ages (in Ma). Data outlines a general cooling between 58.9 ± 7.0 and 39.8 ± 3.0 Ma. Some samples outside of the dome show two age clusters, with an additional age of c. 100 Ma. Additional temperature data refers to zircon fission track ages of (*) Saddiqi et al. (2006), Apatite fission track ages of (Δ) Poupeau et al. (1998) and (+) Mount et al. (1998), and AHe, AFT and ZFT ages of (+, grey) Hansmann et al. (2017). Moreover, the locations of samples used for fluid inclusion measurements are shown. Colors in the background depict geological units (brown: ophiolite, pink: Hawasina units, light green: Muti Fm., dark green: Wasia and Kahmah Gp., blue: Sahtan Gp., purple: Mahil Fm, orange: Saiq Fm, grey: pre-Permian, shaded DEM from Esri, Digital Globe, swisstopo, and the GIS user Community).

Table 2: Results of zircon (U-Th)/He dating.

sample / aliquot	lithology / location	Easting	Northing	He vol. [ncc]	He 1σ [%]	^{238}U mass [ng]	^{238}U 1σ [%]	^{238}U conc. [ppm]	^{232}Th mass [ng]	^{232}Th 1σ [%]	^{232}Th conc. [ppm]	Th/U ratio	Sm mass [ng]	Sm 1σ [%]	Sm conc. [ppm]	ejection correct. (Ft)	uncorr. He age [Ma]	FT He age [Ma]	FT 2σ [%]	FT 2σ [Ma]	mean age [Ma]
T1-Z1	sandstone			5.31	0.83	1.04	1.81	212.00	0.38	2.41	77.66	0.37	0.03	10.43	6.44	0.754	38.90	51.60	8.20	4.20	48.70 +/- 1.80
T1-Z2		547533	2574875	6.05	0.84	1.31	1.81	323.34	0.33	2.41	80.49	0.25	0.01	21.24	2.97	0.737	36.10	49.10	8.70	4.30	
T1-Z3	Fara Fm.		Autochthon A	3.45	0.87	0.84	1.81	212.21	0.30	2.41	74.73	0.35	0.02	14.08	3.83	0.719	31.30	43.60	9.20	4.00	
T1-Z4				3.15	0.86	0.64	1.82	178.10	0.34	2.41	95.86	0.54	0.01	15.61	4.16	0.72	36.30	50.50	9.10	4.60	
T2-Z1	tuffite			9.23	0.83	2.04	1.81	352.85	1.03	2.41	178.16	0.50	0.04	9.53	7.26	0.778	33.40	42.90	7.60	3.20	46.10 +/- 2.00
T2-Z2		547533	2574875	8.58	0.83	1.99	1.81	376.54	0.88	2.41	166.07	0.44	0.07	7.63	14.20	0.757	32.30	42.70	8.10	3.50	
T2-Z3	Fara Fm.		Autochthon A	12.48	0.83	2.32	1.81	377.81	1.01	2.41	163.95	0.43	0.03	11.07	5.44	0.789	40.20	51.00	7.30	3.70	
T2-Z4				6.16	0.83	1.26	1.81	186.92	0.52	2.41	76.65	0.41	0.03	10.98	4.83	0.768	36.80	48.00	7.80	3.80	
T3-Z1	sandstone			3.69	0.86	1.04	1.81	361.71	0.41	2.41	142.73	0.39	0.02	15.90	6.29	0.689	26.90	39.10	10.00	3.90	42.60 +/- 1.70
T3-Z2		544722	2570255	2.82	0.88	0.63	1.82	254.57	0.22	2.42	87.47	0.34	0.02	12.85	9.07	0.694	34.20	49.40	9.90	4.90	
T3-Z3	Muaydin Fm.		Autochthon A	1.54	0.90	0.35	1.85	116.01	0.23	2.42	75.70	0.65	0.02	17.64	5.19	0.67	31.80	47.50	10.50	5.00	
T3-Z4				4.71	0.84	1.20	1.81	309.13	0.70	2.41	180.18	0.58	0.05	9.18	12.12	0.74	28.50	38.50	8.60	3.30	
T3-Z5				8.91	0.83	1.95	1.81	262.57	1.30	2.41	175.08	0.67	0.07	9.00	9.29	0.761	32.60	42.90	8.00	3.40	
T3-Z6				9.80	0.83	2.52	1.81	283.31	1.13	2.41	127.16	0.45	0.06	7.80	6.56	0.816	29.00	35.60	6.60	2.30	
T3-Z7				11.83	0.83	2.41	1.81	219.27	1.23	2.41	111.66	0.51	0.11	7.31	10.01	0.794	36.10	45.50	7.10	3.20	
T3-Z8				8.41	0.83	1.85	1.81	224.86	1.04	2.41	125.92	0.56	0.07	9.09	8.40	0.784	33.10	42.20	7.40	3.10	
T4-Z1	conglomerate			18.23	0.83	1.79	1.81	380.98	0.44	2.41	93.57	0.25	0.02	13.79	3.77	0.736	79.30	107.60	8.70	9.40	93.80 +/- 6.90
T4-Z2		517510	2560808	10.68	0.83	1.36	1.81	392.55	0.35	2.41	100.65	0.26	0.02	15.99	5.30	0.703	61.20	86.90	9.60	8.40	
T4-Z3	Muti Fm.		Autochthon B	5.24	0.85	0.56	1.82	137.78	0.48	2.41	118.23	0.86	0.04	8.48	11.06	0.738	64.20	86.90	8.60	7.50	
T5-Z1	turbiditic sandstone			34.15	0.82	3.38	1.81	502.17	0.79	2.41	117.95	0.23	0.10	7.97	14.16	0.781	78.70	100.80	7.50	7.60	106.00 +/- 5.20
T5-Z2		512934	2561691	13.52	0.83	1.28	1.81	333.42	0.27	2.41	69.42	0.21	0.02	16.57	4.11	0.744	82.70	111.20	8.50	9.50	
T5-Z3	Matbat Fm.		Hawasina N.	8.95	0.83	1.30	1.81	254.43	0.78	2.41	153.35	0.60	0.01	16.47	2.78	0.754	49.70	65.90	8.20	5.40	58.90 +/- 7.00
T5-Z4				9.21	0.84	1.75	1.81	416.93	0.69	2.41	163.29	0.39	0.04	9.44	9.25	0.766	39.80	51.90	7.90	4.10	
T5-Z5				37.88	0.80	51.13	2.33	1.81	561.72	0.37	2.41	90.14	0.16	0.02	11.59	0.741	128.10	172.90	8.60	14.90	
T6-Z1	granodiorite			6.55	0.83	1.00	1.81	241.80	1.28	2.41	311.91	1.29	0.29	5.62	69.36	0.747	41.60	55.60	8.30	4.60	53.70 +/- 1.20
T6-Z2		478301	2592360	6.39	0.85	0.97	1.81	288.96	1.32	2.41	394.16	1.36	0.28	5.31	84.38	0.719	41.10	57.20	9.10	5.20	
T6-Z3	Trondjemite		Semail Ophio.	7.07	0.83	1.06	1.81	314.75	1.79	2.41	528.55	1.68	0.19	5.49	57.19	0.751	39.20	52.30	8.20	4.30	
T6-Z4				12.11	0.84	1.79	1.81	347.26	3.35	2.41	649.55	1.87	0.31	5.55	61.00	0.769	38.60	50.20	7.70	3.80	
T6-Z5				6.78	0.84	1.08	1.81	273.36	1.46	2.41	368.85	1.35	0.27	5.75	68.70	0.738	39.10	53.00	8.60	4.50	
T7-Z1	quarzite			14.91	0.84	1.56	1.81	427.30	0.43	2.41	118.20	0.28	0.05	9.26	12.45	0.744	73.80	99.20	8.50	8.50	99.20
T7-Z2		514817	2586049	4.14	0.87	1.35	1.81	428.75	0.38	2.41	119.50	0.28	0.02	12.47	7.90	0.729	23.70	32.50	8.90	2.90	43.00 +/- 3.70
T7-Z3	Matbat Fm.		Hawasina N.	6.37	0.85	1.33	1.81	274.36	0.30	2.41	62.67	0.23	0.03	10.62	6.71	0.769	37.50	48.80	7.90	3.80	
T7-Z4				9.66	0.81	12.43	2.13	1.81	539.06	0.15	2.45	38.38	0.07	0.01	17.24	0.777	36.90	47.50	7.70	3.70	
T7-Z5				4.03	0.83	5.46	0.94	1.81	232.12	0.47	2.41	115.05	0.50	0.02	12.63	0.738	31.70	43.00	8.60	3.70	
T8-Z1	tuffitic sandstone			4.60	0.86	1.34	1.81	450.89	1.11	2.41	374.66	0.83	0.16	5.81	53.52	0.759	23.70	31.20	8.00	2.50	39.80 +/- 3.00
T8-Z2		532600	2578681	2.92	0.85	0.56	1.82	147.09	0.86	2.41	226.75	1.54	0.28	5.14	73.06	0.715	31.40	44.00	9.20	4.00	
T8-Z3	Mistal Fm.		Autochthon A	2.21	0.89	0.46	1.83	168.48	0.57	2.41	208.48	1.24	0.05	8.65	16.66	0.716	30.90	43.20	9.20	4.00	
T8-Z4				3.46	0.85	0.85	1.81	212.57	0.41	2.41	103.10	0.49	0.01	14.27	3.65	0.74	30.30	41.00	8.60	3.50	
T9-Z1	quarzite			2.90	0.86	0.61	1.82	238.35	0.50	2.41	198.12	0.83	0.01	16.09	5.23	0.705	33.10	46.90	9.50	4.50	45.50 +/- 2.40
T9-Z2		532595	2568258	0.72	0.98	0.18	1.94	109.52	0.13	2.43	76.58	0.70	0.05	10.52	29.38	0.674	27.50	40.80	10.50	4.30	
T9-Z3	Mistal Fm.		Autochthon A	2.04	0.89	0.41	1.84	147.39	0.28	2.41	101.51	0.69	0.01	18.70	3.60	0.718	35.10	48.80	9.20	4.50	
T10-Z1	sandstone			5.09	0.85	0.93	1.81	213.39	0.95	2.41	217.83	1.02	0.02	13.41	4.93	0.754	36.40	48.20	8.10	3.90	46.90 +/- 4.10
T10-Z2		534779	2572636	6.71	0.83	1.37	1.81	267.61	1.24	2.41	241.07	0.90	0.04	9.18	8.32	0.763	33.30	43.70	7.90	3.40	
T10-Z3	Mistal Fm.		Autochthon A	8.97	0.83	2.25	1.81	568.33	1.79	2.41	452.52	0.80	0.04	8.74	10.22	0.723	27.70	38.40	9.00	3.50	
T10-Z4				2.26	0.88	0.35	1.85	118.10	0.39	2.41	131.18	1.11	0.02	14.08	5.39	0.727	41.80	57.50	8.90	5.10	
T11-Z1	quarzite			4.70	0.84	1.01	1.81	188.02	0.57	2.41	106.02	0.56	0.01	19.39	2.18	0.746	34.00	45.60	8.40	3.80	42.50 +/- 2.00
T11-Z2		540394	2572230	1.55	0.90	0.39	1.84	109.55	0.33	2.41	93.99	0.86	0.01	20.85	2.31	0.706	27.30	38.80	17.60	6.80	
T11-Z3	Mistal Fm.		Autochthon A	1.50	0.94	0.37	1.84	110.19	0.19	2.42	56.69	0.51	0.01	17.25	3.39	0.693	29.90	43.20	9.90	4.30	
T12-Z1	sandstone			5.35	0.85	1.21	1.81	355.93	1.09	2.41	320.43	0.90	0.02	16.47	5.58	0.706	30.10	42.70	9.50	4.00	40.10 +/- 1.50
T12-Z2		531776	2582871	4.28	0.86	1.12	1.81	286.68	0.16	2.42	40.59	0.14	0.01	27.93	1.79	0.736	30.70	41.70	8.80	3.70	
T12-Z3	Sahtan Gp.		Autochthon B	3.80	0.86	1.06	1.81	349.54	0.14	2.43	44.41	0.13	0.01	22.03	2.70	0.719	28.70	39.90	9.20	3.70	
T12-Z4				1.51	0.89	0.38	1.84	92.50	0.32	2.41	76.60	0.83	0.01	15.61	3.53	0.758	27.30	36.10	8.10	2.90	

374

375   These ages indicate a large-scale cooling signal that affects the entire Jebel Akhdar area; the ZHe age pattern and

376   1D thermal models indicate a phase of rapid cooling below 170 °C in the early Cenozoic (58.9 ± 7.0 and

377   39.8 ± 3.0 Ma). The range of modeled cooling paths outline maximum cooling rates of 2-8 °C/Myr. This is

378   followed by slower cooling until the present day.

379   Data from the Muti Fm. and the Hawasina units differ partly from this trend: the apparent ZHe ages of clasts in

380   the Muti sample T4 (mean: 93.8 ± 6.9 Ma) is as old as its respective stratigraphic age (Robertson, 1987). Even

381   though all ages reproduce within error, this indicates partial reset of the ZHe system, as post-depositional reheating

382   above closure temperature would result in younger ages. Samples of the lower Hawasina Nappes contain two grain

383   age clusters. Older ages coincide with higher uranium concentrations suggesting that only the younger ages

384   represent thermally reset zircons. We note that the older ZHe ages of 110-95 Ma coincide with timing of forebulge

385   migration through the area, as independently determined in the stratigraphic record by the Wasia-Aruma Break

386   (Figure 3). This may be either pure coincidence, due to partial resetting of an older grain age population, or may

387   be a grain age population with higher closure temperature witnessing exhumation. We discuss reasons for different

388   resetting temperatures below. However, partial reset of ZHe ages suggests that the Hawasina samples have not

389   experienced temperatures exceeding the partial retention zone (PRZ) of 130-170 °C.

390   A sample from an intrusive body of the Semail Ophiolite yields ZHe ages of 53.7 ± 1.2 Ma (T6) with a modeled

391   cooling path gradually decreasing into the PRZ until c. 55 Ma. This time interval of passing the PRZ is comparable

392   to the Hawasina nappe samples beneath the ophiolite but occurs slightly earlier than cooling of the Autochthonous.

393   Nevertheless, Semail Ophiolite, Hawasina Nappes and the autochthonous margin sequence were affected by the

394   same cooling event that was possibly initiated by exhumation of the Jebel Akhdar Dome.

395   **4.3.   Fluid inclusions**

396   The Muti veins' samples FI-M1 and M2 of the southern Jebel Akhdar show evidence of crack and seal processes

397   (youngest parts in the center of the vein, Ma-2010-11b and 14a of Arndt 2015) with blocky quartz grains that

398   contain two kinds of roundish primary FIs with sizes of 3-20 µm. They are mainly aligned along dark zones and

399   are interpreted as growth zones or form bright clusters in the central part of the crystals. A third set of fluid

400   inclusions (FIs) appears in large, grain-crosscutting trails interpreted to be of secondary origin. Calcite crystals

401   within the Natih veins contain bright FIs with sizes of 2-20 µm and are edgy, often rectangular or trapezoidal in

402   shape. Identified primary FIs are aligned parallel to crystal growth zones.

403   All measured FIs are two-phase, liquid-vapor inclusions with ice as last phase to melt. The Muti samples show

404    $T_{fm(ice)}$ between -5.1 ± 0.5 and -4.6 ± 0.3 °C and $T_{m(ice)}$ at -2.2 ± 0.2 to -1.9 ± 0.1 °C, the Natih sample T_{fm} of -

405   18.4 ± 1.9 to -20.2 ± 2.1 °C and $T_{m(ice)}$ of -7.1 ± 0.3 to -8.9 ± 1.8 °C (Table 3). First melting temperatures of all

406   inclusions correspond to an H_2O-NaCl system and complete melting temperatures of ice indicate salinities similar

407   to seawater (3.0 ± 0.5 to 3.5 ± 0.3 wt.-% NaCl eq., Muti Fm., Figure S6) or three times higher (10.3 ± 0.3 to

408   12.5 ± 2.0 wt.-% NaCl eq., Natih Fm., Figure S6).

409   **Table 3: Results of FI microthermometry. Identified FI types, their measured homogenization temperatures and results**
410   **of the pressure correction for 280 and 340 MPa accounting for 8 and 10 km of ophiolite with partly serpentinized mantle**
411   **sequence and 2 km of Hawasina nappes, and for 45 MPa accounting for 2 km of sedimentary overburden for samples**
412   **unaffected by ophiolite obduction. First melting (T_{fm}) and final melting of ice ($T_{m\ ice}$) temperatures and salinities are**
413   **given. Data by Holland et al. (2009) are added for comparison and we likewise corrected their homogenization**
414   **temperatures. (* further heating was avoided to prevent fluid inclusion damage)**

sample No.	vein orient., location and host mineral	FI kind	No. of FIA	T_h [°C]	pressure corrected T [°C] for 45 MPa		T_{fm} [°C]	$T_{m\,ice}$ [°C]	salinity [wt.-% NaCl]
FI-M1	NE-SW striking	primary	21	166 +/- 7	189 +/- 7		-4.7 +/- 0.2	-2.2 +/- 0.2	3.5 +/- 0.3
	strike-slip vein (IX), Muti Fm.	primary	22	189 +/- 3	213 +/- 3		-4.6 +/- 0.3	-2.0 +/- 0.3	3.2 +/- 0.4
	Gorge area, quartz	secondary	18	> 200*	> 224		-4.6 +/- 0.2	-2.0 +/- 0	3.2 +/- 0
					pressure corrected T [°C] for 45 MPa				
FI-M2	NE-SW striking	primary	24	161 +/- 3	184 +/- 3		-5.1 +/- 0.5	-1.9 +/- 0.1	3.0 +/- 0.2
	strike-slip vein (IX), Muti Fm.	secondary	12	116 +/- 12	138 +/- 12		-	-	-
	Gorge area, quartz	secondary	24	150 +/- 2	172 +/- 2		-	-	-
					for 280 MPa	for 340 MPa			
FI-N1	Natih Fm., NW-SE	primary	14	90 +/- 5	235 +/- 5	266 +/- 5	-18.4 +/- 1.9	-7.1 +/- 0.3	10.3 +/- 0.3
	burial vein (III), Wadi Nakhr, calcite	primary	26	(114 +/- 7)	(264 +/- 7)	(297 +/- 7)	-20.2 +/- 2.1	-8.9 +/- 1.8	12.5 +/- 2.0
FI-N2	Natih Fm., early E-W vein (I) Al Raheba, calcite	primary	10	80 +/- 4	225 +/- 4	256 +/- 4	-	-	-
					for 280 MPa	for 340 MPa			
Holland et al. (2009)	Sahtan Gp., bedding parallel shear vein, top-to-NE (IV), Wadi Nakhr, quartz	primary and pseudosec.	n.a.	134-141	296-303	357-364	from -19	-3.7 to -2.3	3.8 to 6.0

Primary inclusions in quartz crystals from the Muti Fm. show minimum trapping temperatures of 161 ± 3 to 166 ± 7 °C (Table 3, FI-M2 and middle of FI-M1) with a second primary population of 189 ± 3 °C (sides of vein FI-M1). T_h of secondary inclusions in FI-M1 are above 200 °C. In sample FI-M2, two generations of secondary inclusions were observed, both reflecting lower T_h than the primary inclusions. No hints of necking down, leakage or stretching were observed at the measured inclusions and over 90 % of the measured FIs in one assemblage are in the range of 10-15 °C representing a good quality of the measurements (Goldstein, 2001).

Samples FI-N1 and N2 of the Natih Fm. in the southern Jebel Akhdar (Figure 4) contain primary inclusions hosted by calcite crystals giving T_h of 80 ± 4, 90 ± 5 and 114 ± 7 °C (Table 3). The latter population is often characterized by elongated, possibly stretched FI, and is not considered for further interpretations. Assuming vein formation during burial (Grobe et al., 2018; Hilgers et al., 2006; Holland et al., 2009a; Virgo, 2015) under 8 to 10 km of ophiolite including partially serpentinized peridotite and 2 km of Hawasina Nappes, results were pressure corrected for 280 and 340 MPa leading to corrected homogenization temperatures of 235 ± 5 and 266 ± 5 °C (FI-N1), and 225 ± 4 and 256 ± 4 °C (FI-N2, Table 3). Signs of strong deformation such as twinning or cleavage were not observed in the measured inclusions; secondary inclusions were present but not measured.

These temperatures represent minimum trapping conditions of a paleo-fluid and do not necessarily represent burial temperatures of the host rock. It should be noted that the analyzed Natih veins formed bedding confined (Grobe et al., 2018; Holland et al., 2009a; Virgo, 2015) and show host rock buffered carbonate isotope signatures (Arndt et al., 2014; Hilgers et al., 2006). This corroborates the idea that analyzed veins were in thermal equilibrium with their host rocks.

FI microthermometry of late strike-slip veins in the Muti Fm. are interpreted to have formed after dome formation (Grobe et al., 2018; Virgo, 2015) at an assumed minimum depth of 2 km (preserved allochthonous thickness). A pressure correction for the related 45 MPa corresponds to minimum fluid trapping temperatures of 184 ± 3 °C (FI-

438 M2) and 213 ± 3 °C (FI-M1) with a later phase of primary inclusions outlining 189 ± 7 °C and even cooler

439 secondary inclusions of 138 ± 12 to 172 ± 2 °C (FI-M1 and M2, Table 3). These cooler fluid temperatures can be

440 explained by further exhumation of the Jebel Akhdar and, hence, cooling of the fluids' reservoir during crack-seal

441 vein formation. Isotope studies on the vein calcite do not support an open system with fluid exchange (Stenhouse,

442 2014; Virgo and Arndt, 2010), hence, we interpret the formation of strike-slip related veins as having formed

443 during exhumation following peak burial.

444 Based on the assumption that fluid and host rock were in thermal equilibrium, we can use maturity data in

445 combination with fluid inclusion data to estimate the pressure at vein formation. Peak temperatures of the Sahtan

446 Group revealed by RSCM reached 283 ± 9 to 286 ± 6 °C (Table 1, Figure 5 red line) and enable to solve the

447 pressure-temperature couples of FIs measured in Sahtan veins formed at deepest burial by Holland et al. (2009,

448 black line). This results in minimum trapping pressures of 254 ± 30 MPa at times of vein formation (Figure 5 blue

449 line), which correspond to times close to or at deepest burial of the carbonate platform.
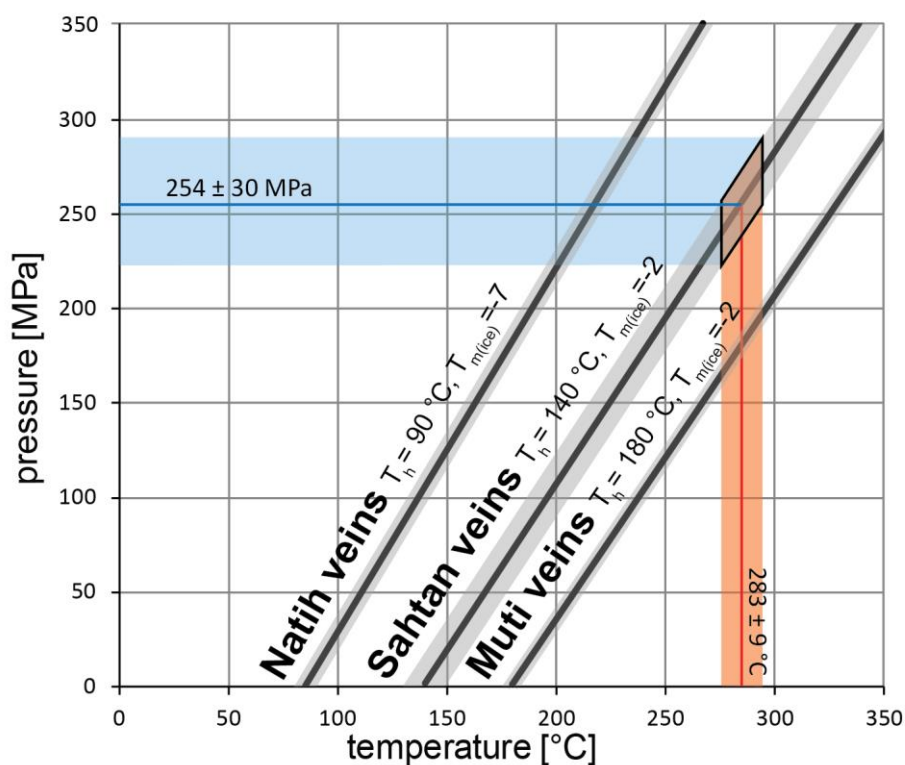
450

451 **Figure 5: Fluid inclusion isochores (solid black lines) of analyzed fluid inclusion populations with corresponding std.**
452 **deviations (shaded areas, for Sahtan Group data of Holland et al., 2009, conservatively ± 10°C are assumed). To estimate**
453 **the pressure conditions during vein formation, calculated temperatures from thermal maturity data are added for the**
454 **Sahtan Group (red line with error) and result in minimum trapping pressures of 254 ± 30 MPa during peak burial (blue**
455 **line with error).**

456 **4.4.   Basin modeling**

457 Numerical basin modeling integrates all data and tests the individual interpretations in the thermal and geodynamic

458 framework. Deepest burial was constrained with thermal maturity data and exhumation with thermochronological

459 data. In the following we present our best fit model, considering a mixed ophiolite lithology (Searle and Cox,

460 2002) consisting of strongly serpentinized peridotites. Then, the sensitivity of important results to changes of

461 relevant input parameters are discussed.

462 Modeled evolution of the transect over time is given in Figures 6 and 7, showing (a) final deposition of the
463 Autochthonous B, (b) erosion of the Natih Fm. in the North by a moving foredeep (no erosion in S, full erosion in
464 N), (c) emplacement of 1400 m of Hawasina Nappes, and d-e) ophiolite obduction reconstructed by rapid, stepwise
465 sedimentation. After maximum burial beneath the ophiolite complex at c. 80 Ma (Warren et al., 2005) exhumation
466 is assumed to start slightly prior to 55 Ma (Saddiqi et al., 2006) with a rapid phase of cooling below c. 200 °C at
467 55 Ma leading to lower temperatures in the Jebel Akhdar region. 1D burial plots of two pseudo-wells created out
468 of point data in Wadi Nakhr and Wadi Yiqah are shown in Figure 8.

469
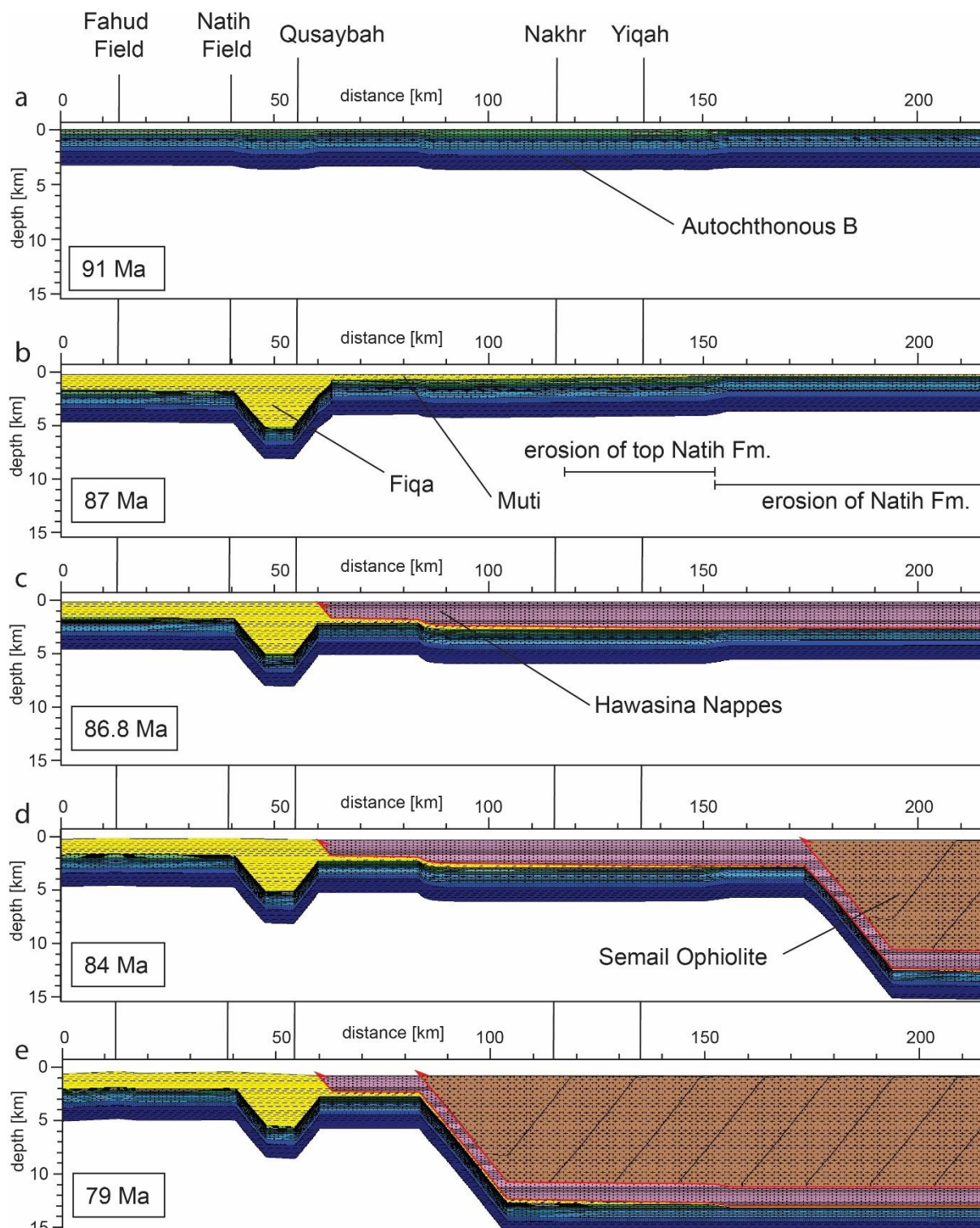
470

471 **Figure 6: Modeling results: Transect evolution from sedimentation of the Autochthonous B at stable passive margin**
472 **conditions (a), to moving foredeep that finally filled with Fiqa sediments (b, peak burial as calibrated by thermal**
473 **maturity data), Hawasina Nappe (c) and ophiolite emplacement (d) leading to deepest burial (e). Highlighted with**
474 **vertical lines in the background are the locations of present-day oil fields and sampled valley locations. Please note the**
475 **unrealistically flat topography which is a result of the modelling set-up.**

476
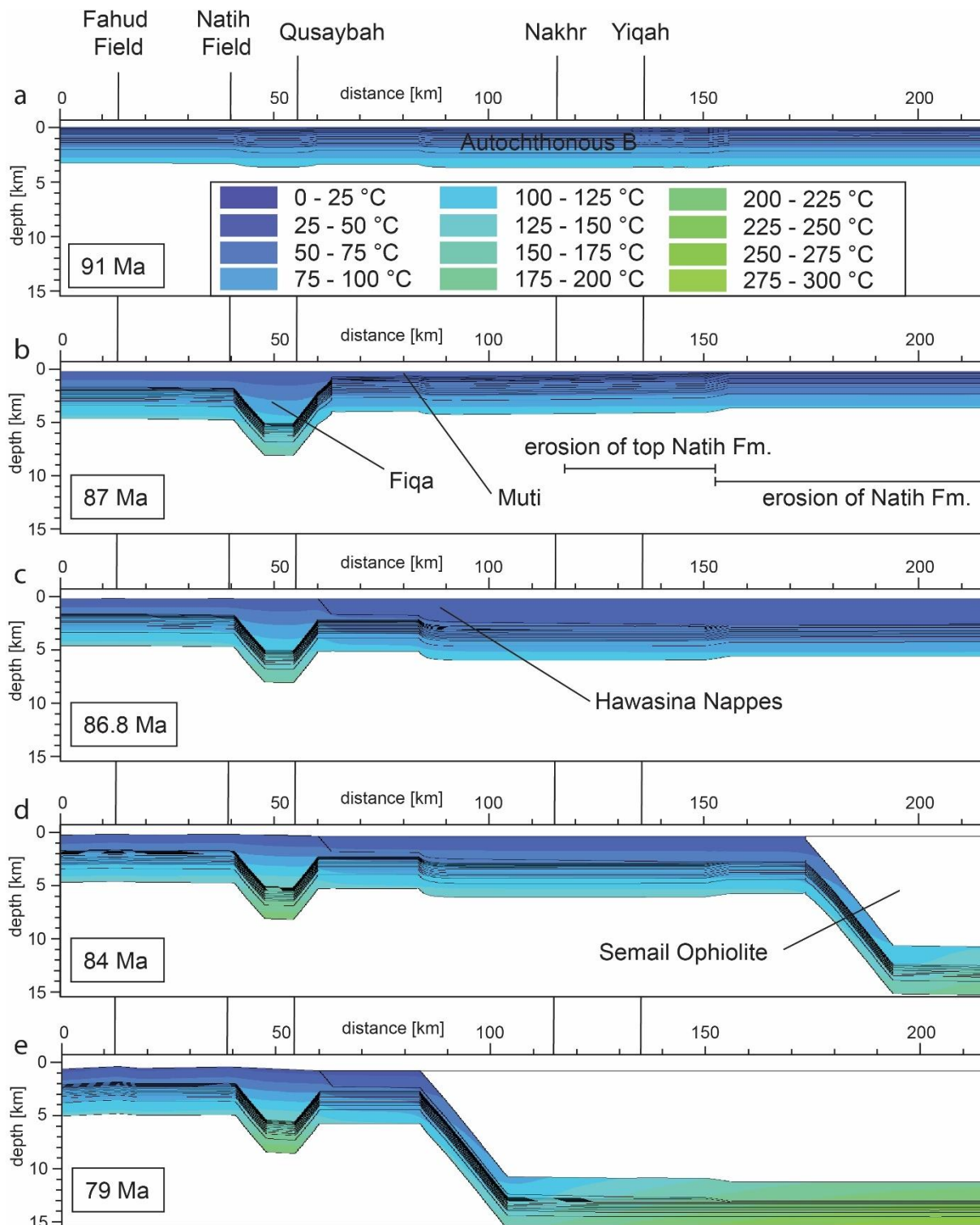
478 **Figure 7: Modeling results: Temperature distribution and temporal evolution along the transect of Figure 6.**
479 **Highlighted with vertical lines in the background are the locations of present-day oil fields and sampled valley locations.**

480
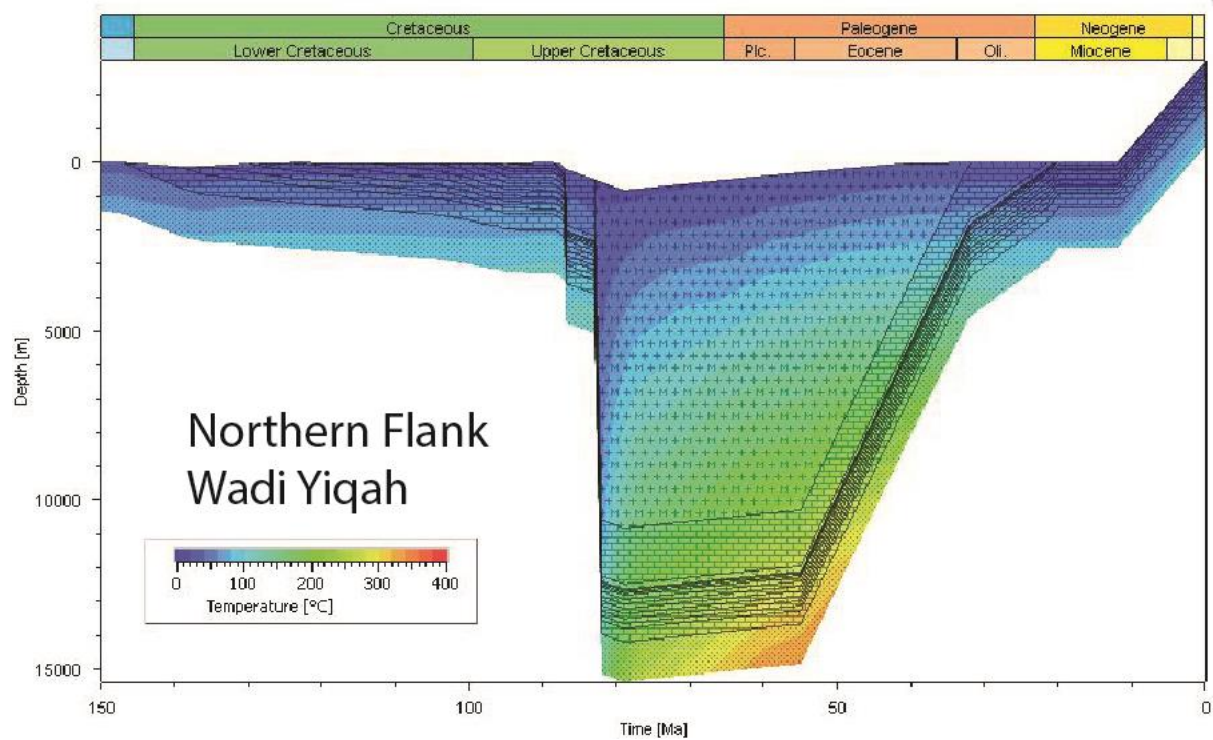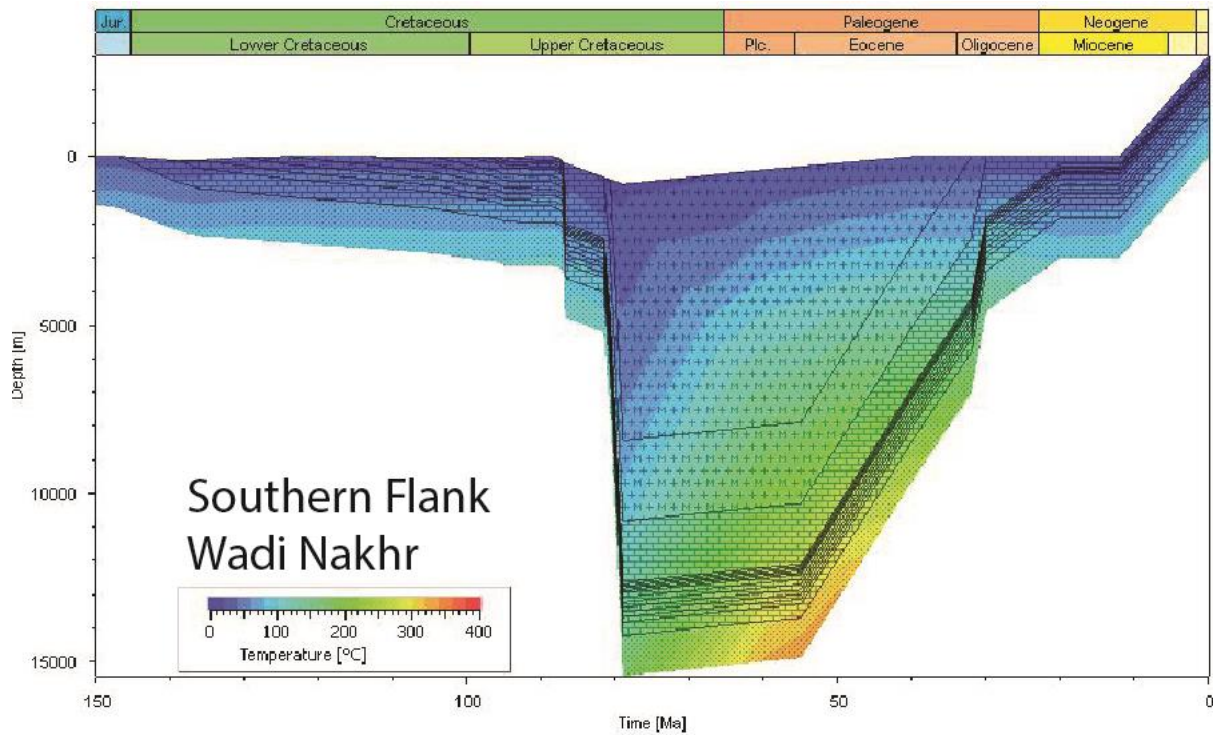
Figure 8 Modeling results: Two representative burial plots for two pseudo-wells created near the entrances of Wadi Nakhr and Yiqah (Figures 1, 6 and 7) show two phases of rapid burial related to Hawasina and Semail Nappe emplacement and c. 88 Ma and ophiolite emplacement at c. 78 Ma. Burial in the North (Wadi Yiqah) starts c. 2 Myr earlier due to ophiolite obduction taking place from N to S.

As a model set up only presents one possible solution out of several, sensitivity analyses with varying paleo-overburden thicknesses (Figures 9 and 10), changing degree of serpentinization of the ophiolite and varying basal heat flow during deepest burial (Figure 11) are presented and discussed below.

488 Thermal maturity data of the Natih B at Jebel Qusaybah (1.1 % VR$_r$), Adam Foothills, require peak temperatures

489 of c. 140 °C (Table 1). Sensitivity analyses of the overburden above the Natih Fm. show that maximum 4 km of

490 sedimentary overburden (Figures 9a and 10a) is needed to match the calibration data (Figures 9a and 10a).

491
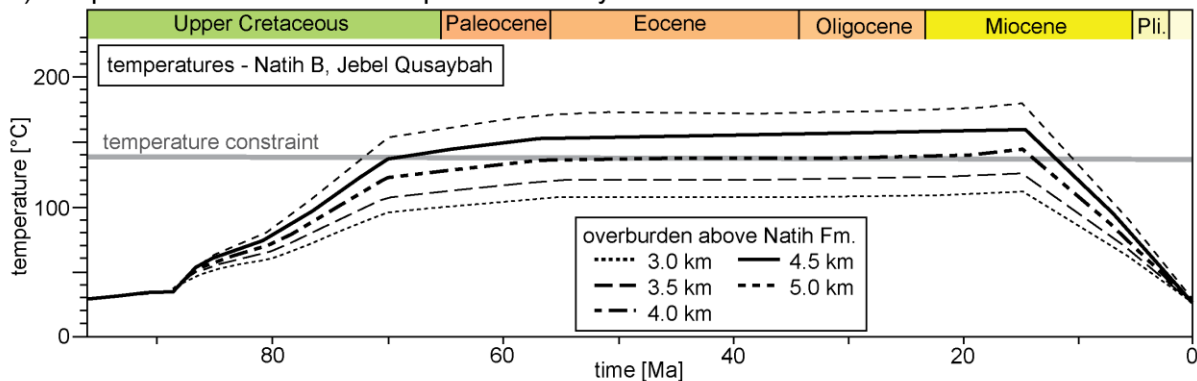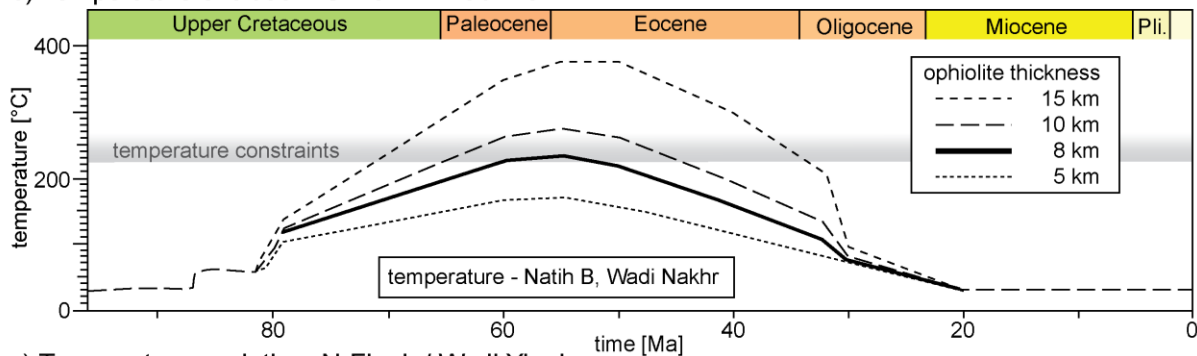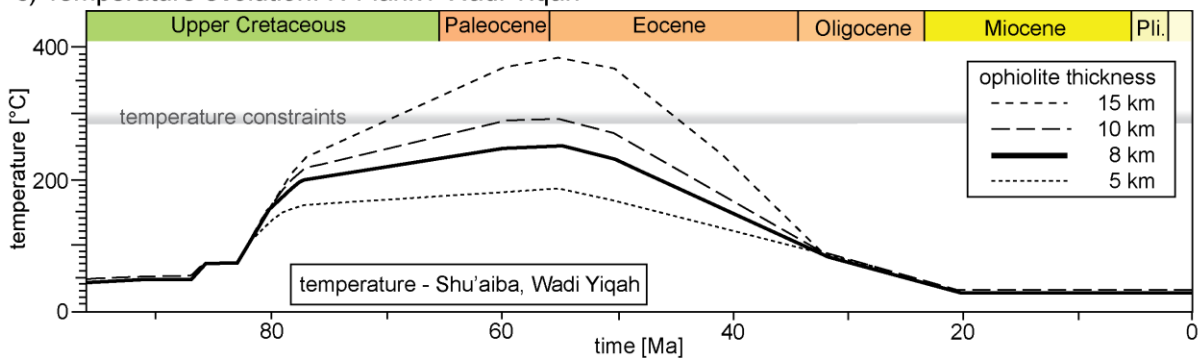
492

493 **Figure 9: Sensitivity analysis of paleo-overburden and its influences on temperature in comparison to calculated peak**
494 **temperatures (gray area) for pseudo-wells at Jebel Qusaybah (a), Wadi Nakhr (b) and Wadi Yiqah (c).**
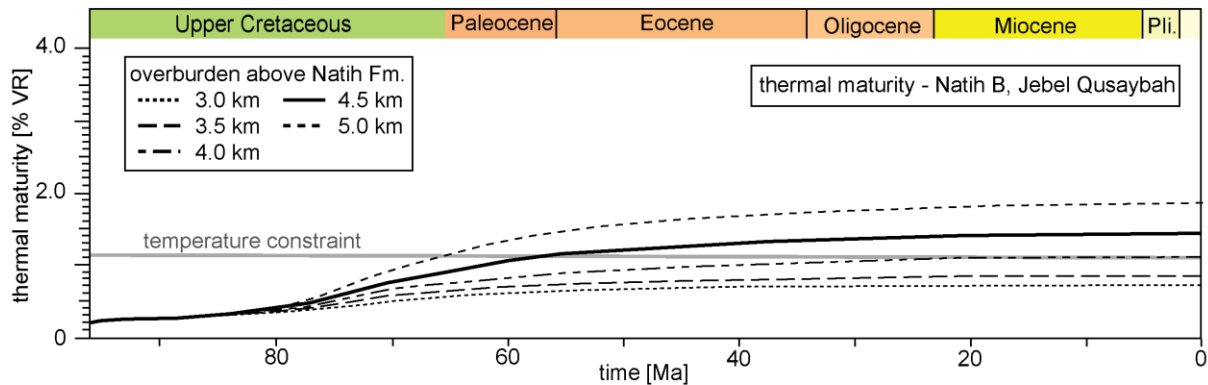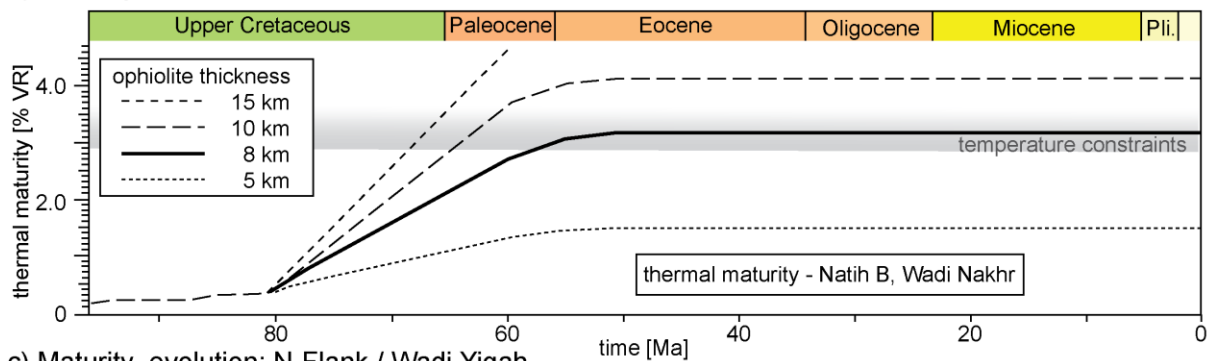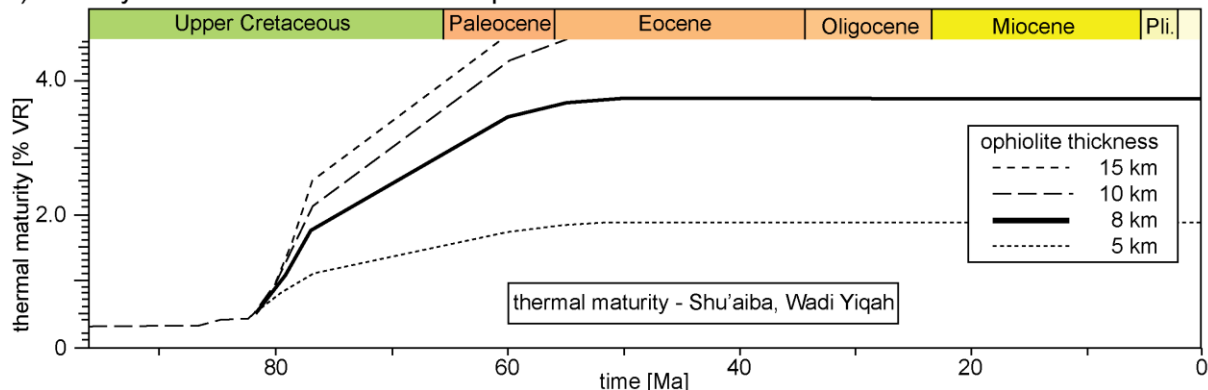
Figure 10: Sensitivity analysis of paleo-overburden and its influences on thermal maturity in comparison to calibration data (gray area). Data is used to calibrate burial depth of the foredeep at the Jebel Qusaybah (a) and the paleo-ophiolite thickness at the southern flank of the Mountains at Nakhr (b). Its northern counterpart at Yiqah (c) is in agreement with the temperature data of Figure 9, however to mature to be reconstructed by standard maturity modelling (Sweeney and Burnham, 1990).

To restore the former minimum thickness of the Semail Ophiolite, the thickness of the Hawasina Nappes along the transect was fixed to 2 km, as suggested by the maximum present-day thickness of the Jebel Misht exotics. To reach the required thermal conditions measured at the entrance of the Wadi Nakhr (Natih B: 2.83-3.72 % VR_r, 225-260 °C; Grobe et al., 2016), 8-10 km of original, total thickness of strongly serpentinized ophiolite sequence are needed in addition to the 2 km of Hawasina Nappes (Figures 9b and 10b). These thicknesses are also sufficient to reach peak temperatures calculated for older stratigraphy at the northern flank of the Jebel Akhdar Dome (Shu'aiba Fm. at Wadi Yiqah: 270-295 °C by RSCM, Figures 9c and 10c). Modeling results show an earlier heating and more rapid increase in maturity in the north. We associate this with the 2 Mys earlier onset of obduction and, hence, a longer burial of the northern carbonate platform (Wadi Yiqah) under the active ophiolite obduction compared to is southern counterpart (Béchennec et al., 1990; Cowan et al., 2014).

511   Another factor influencing the modeling results is related to the lithology of the overburden and its compaction.
512   In the special case of burial under an ophiolite, serpentinization of peridotite and its impact on ophiolite density
513   and thermal conductivity must be considered. Sensitivity analysis of ophiolite serpentinization shows the
514   temperature and thermal maturity effects on our model (Figure 11). A model-case of ophiolite without any
515   serpentinized peridotite (0 %-case, ρ_{ophio}=3133 kg/m³) would represent the largest deviation compared to our best-
516   case model assuming complete ophiolite serpentinization (100 %-case, ρ_{ophio}=3069 kg/m³). This density is based
517   on Al-Lazki et al. (2002). Even if the upper part of the ophiolite was missing in the Jebel Akhdar area (Nicolas
518   and Boudier, 2015), this and the field data of Searle and Cox (2002) in the Saih Hatat support strong
519   serpentinization. A less serpentinized ophiolite means higher densities and related higher thermal conductivities
520   of the overburden and thus lower peak temperatures in the sediments below. In the case of no serpentinization,
521   peak temperature of Natih B in the Wadi Nakhr would decrease by c. 60 °C resulting in a maximum thermal
522   maturity decrease of 1.5 % VR. The best fit model with an ophiolite thickness of 8-10 km would need additional
523   3 km of overburden at 0 % serpentinization to equally match the measured thermal maturities. Additional
524   thicknesses of 0.75 km (75 % serpentinization), 1.5 km (50 % serpentinization) and 2.25 km (25 %
525   serpentinization) apply for lower degrees of serpentinization, respectively (compare Fig. 9).
526   Results depend strongly on basal heat flow (Figure S3). The best fit model of 40 mW/m² at maximum burial is
527   typical for a passive continental margin setting. If this heat flow at peak burial would be lowered to 30 mW/m² an
528   additional amount of 1.2 km of ophiolitic overburden would be required to achieve a match with thermal
529   calibration data (Figure 11). Increased heat flow values to 50, 60 or 70 mW/m² would result in lowering of
530   overburden by 1.3, 2.4 and 3.5 km, respectively (Figure 11).
531
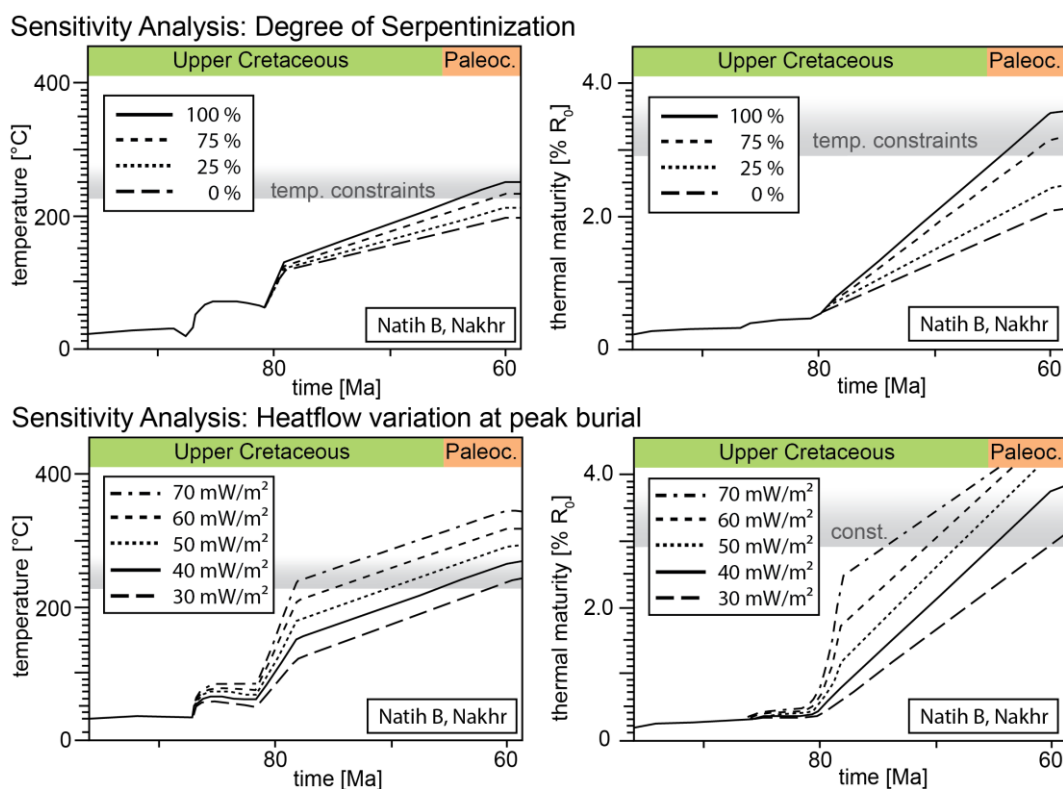
533   **Figure 11: Sensitivity analysis: Top: Different degrees of serpentinization of the peridotite within the Semail Ophiolite**
534   **affect the temperature (left) and thermal maturity (right) evolution (modeled for Natih B Fm. at Wadi Nakhr). Pure**
535   **peridotite (0 % serpentinization) require additional 3 km of ophiolite in addition to the 8-10 km of the best-fit model to**
536   **equally match the calibration data. 100 % refers to complete serpentinization of the peridotite in the ophiolite. Bottom:**
537   **The influence of variable heat flow values at peak burial on temperature (left) and thermal maturity (right).**

5. Discussion

Evaluating uncertainties in basin and petroleum system models is especially important for complex areas such as the Jebel Akhdar, where sedimentary rocks reached high temperatures and maturities due to deep and rapid burial. In the following, we discuss these uncertainties with respect to temperature and burial history, overpressure build-up and induced fluid flow. For all presented basin models of the study area, the following assumptions apply: (1) decompacting the present-day lithologies does not consider rock volume lost by pressure solution. This is probably of minor importance in our study area as host-rock buffered isotope ratios of the veins were interpreted as local sinks for nearby dissolved calcite (Arndt et al., 2014; Hilgers et al., 2006), so that the overall rock volume remains approximately constant, (2) decompaction only accounts for burial, whereas a possible tectonic compaction is neglected (Neumaier, 2015) and (3) calculated overpressure does not include a rock volume decrease due to pressure solution.

5.1. Burial history

Little is known about the very early phase of burial, before 91 Ma (Figures 6 and 7, Grobe et al., 2018). The assumptions for this period are based on hypotheses on the tectonic evolution of the passive continental margin as well as data on thickness of sedimentary units but are not strongly constrained by geological data.

In Turonian times (Robertson, 1987) a southwest-ward-moving forebulge, related to plate convergence, affected northern Oman. It eroded the northeastern platform edge and migrated southwest-ward to the present-day position of the Adam Foothills (Robertson, 1987). Measured thermal maturities of 1.1 % VR_r were used to reconstruct peak temperatures during burial in Jebel Qusaybah, Adam Foothills to c. 140 °C. Numerical basin modeling results reveal that additional paleo-overburden of maximum 4 km (Natih B, Qusaybah, Figure 10) is required to reach these temperatures. The exhumation history of the Adam Foothills is not well known; our model is based on an interpreted late exhumation during the Miocene (Claringbould et al., 2013). Earlier exhumation would shorten the time span of the rock at higher temperatures (Figure 7), lead to decreased thermal maturity and, hence, would require additional overburden to match the measured thermal maturity data. Therefore, the resulting burial of 4 to 4.5 km has to be regarded as minimum value. South of the Adam Foothills basin geometries do not show tilting and are interpreted as not affected by the moving foredeep. Here peak burial was reached under c. 3 km of Fiqa, Hadhramaut and Fars formations. This is based on the assumption that present-day burial equals deepest burial as no thermal calibration data of the area south of Jebel Qusaybah are available, which is in agreement with interpretations of Terken (1999) and Warburton et al. (1990).

In case of the Jebel Akhdar, peak temperatures were reached as a consequence of burial below the ophiolite (Loosveld et al., 1996; Searle et al., 2003; Searle, 2007; Warren et al., 2005). Here the sedimentary rocks reached high temperatures and maturities as shown by solid bitumen reflectance, RSCM, FT-IR and Rock-Eval pyrolysis data (Fink et al., 2015; Grobe et al., 2016). Pre-obduction burial by sedimentation is not sufficient for such high thermal maturities, and it likewise cannot be explained by increased basal heat flow before 91 Ma or after 55 Ma. Influence of local hydrothermal effects cannot be excluded, but because the entire Jebel Akhdar reached high temperatures, short-term, local events are unlikely to have been dominant. A regional thermal overprint on the passive margin sediments by warm ophiolite obduction can be excluded and is hence not accounted for in the model. Due to the at least 2 km thick imbricated Hawasina Nappes between the ophiolite and the passive margin sequence, the thermal overprint did not affect the top of the carbonate platform. Limited thermal overprint of the units underlying the ophiolite is supported by the fact that the sediments of the nappes directly below the ophiolite

do not show signs of regional metamorphism in the Jebel Akhdar region (Searle, 1985). Moreover, the thermal imprint as observed by the metamorphic sole in northern Oman only affects 10's of meters in the sub-thrust Hawasina Nappes (Searle and Cox, 2002) and not the carbonate platform sediments below. This minor overprint is also observed in other areas (e.g. Wygrala, 1989).

To reach the measured maturity values in the Jebel Akhdar, a paleo-thickness of the ophiolite in the order of 8-10 km on top of 2 km of Hawasina Nappes is required (Figure 10); this corresponds to 280 to 340 MPa of lithostatic pressure, in rough agreement with the pressure reconstructed by combining fluid inclusion data and independently determined thermal rock maturity temperatures (cf. FI results: 254 ± 30 MPa).

Basin modeling indicates that highest temperatures were reached later than deepest burial under the ophiolite (Figure 7), directly prior to exhumation. This difference is interpreted as the time advection needs to heat the rock. Deep burial under the ophiolite represents the only time in the basin's evolution when ductile limestone deformation was possible (Grobe et al., 2018). However, there is uncertainty concerning the exact timing of deepest burial in the Jebel Akhdar (we used 79 Ma according to U-Pb dating of eclogites in the Saih Hatat window; Warren et al., 2005), the related basal heat flow (discussion, Fig. S2) and the beginning of early exhumation (we used 55 Ma, as discussed below). A later exhumation would not be sufficient to match observed thermal maturities with thermometry data. The slightly higher temperatures of the model compared to thermometry data suggest that an even quicker exhumation might have taken place.

Our peak temperatures are in agreement with temperatures of c. 200 °C suggested for the top of the carbonate platform by Breton et al. (2004), non-reset zircon fission tracks in the pre-Permian basement indicating peak temperatures up to 280 °C (Saddiqi et al., 2006), and ductile limestone conditions observed at the Jurassic-Cretaceous boundary (Grobe et al., 2018, Figure 7). Moreover, thermal maturities of the same stratigraphic units show similar values along the transect and around the dome (Grobe et al., 2016). Hence, we assume a similar burial history for the entire Jebel Akhdar and were able to refine previous models (Grobe et al., 2016) with the here presented larger dataset. The temperatures used in our models are in contrast with recent results on mixed layers illite-smectite and clay mineral assemblages from the Jebel Akhdar by Aldega et al. (2017) who argue for peak temperatures of 150-200 °C on the northern flank of the Jebel Akhdar and 120-150 °C on the southern flank. These values are incompatible with our solid bitumen and Raman spectroscopy data, as well as with the overmature Natih B source rock on the southern flank (data presented here and in Grobe et al., 2016). Independent data on temperatures from fluid inclusions confirm the higher temperature range. At present, there is no clear explanation for this discrepancy. However, it has been shown that the vitrinite reflectance system is more sensitive to rapid temperature changes than clay mineralogy (e.g. Hillier et al., 1995; Velde and Lanson, 1993). If burial was short enough, the clay minerals may not have time to recrystallize, possibly due to a lack of potassium, whereas vitrinite reflectance increases. Alternatively, we speculate that the clay minerals were transformed during top-to-NNE shearing, thus their state do not show peak burial. Indeed it has been shown that deformation associated with this early extension reaches deeply into the passive margin sequence, and includes the Rayda and Shuaiba Formations (Grobe et al., 2018; Mattern and Scharf, 2018). Furthermore, Aldega et al. (2017) argue that the cooling history proposed by Grobe et al. (2016) indicates temperature in the basement < 70°C during the Eocene-Oligocene, thus not accounting for thermochronological data in pre-Permian basement rocks. In fact, the calibration data we used for the basement indicate rapid cooling at 55 ± 5 Ma (Poupeau et al., 1998; Saddiqi et al., 2006), in agreement with models of Grobe et al. (2016) and the exhumation presented in this work.

618 This exhumation might be a result of the ductile top-to-NNE shearing event (64 ± 4 Ma, Hansman et al., 2018;
619 Grobe et al., 2018). Its onset marks the exhumation of the carbonate platform after deepest burial. Related peak
620 temperatures measured in fluid inclusions of bedding parallel veins were estimated to 186-221 °C by Holland et
621 al. (2009) assuming an ophiolitic overburden of 5 km (Sahtan Fm., Wadi Nakhr). If we adjust this pressure
622 correction for higher values of 280 to 340 MPa accounting for the here elaborated 8 to 10 km of ophiolite and
623 2 km of sedimentary nappes, trapping temperatures would increase to c. 296-364 °C (Table 3), which are in the
624 order of the maximum burial temperatures as deduced from organic matter maturity.

625 Figure 12 presents a summary burial graph integrating all presented data in a plot of the temperature evolution
626 over time. Additional pressure data is gained by fluid inclusion thermometry: These data indicate paleo-fluid
627 temperatures in the range of 225 ± 4 °C (280 MPa) to 266 ± 5 °C (340 MPa) during burial under the ophiolite
628 (bedding-confined veins), c. 296-364 °C at peak burial (top-to-NNE sheared veins) and 213 ± 3 °C during
629 exhumation with a later phase of primary inclusion outlining 184 ± 3 to 189 ± 7 °C (both strike-slip related veins).
630 Temperature decrease within the latter formed parts of the strike-slip veins might relate to a change of fluid source
631 or to exhumation during vein formation. In combination with our thermochronology data the second possibility
632 appears more likely and would imply strike-slip faults developed after c. 55 Ma.
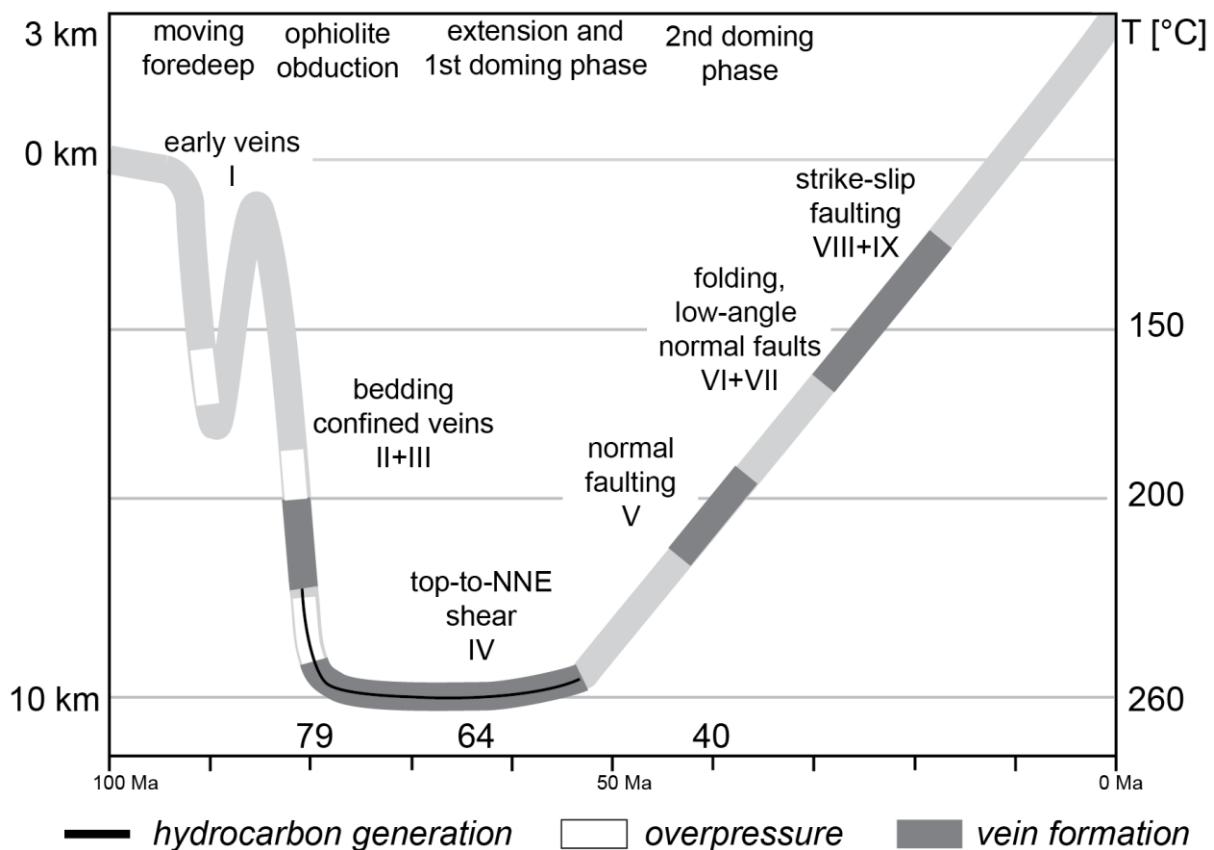
Figure 12: Summary sketch of burial and exhumation for the top of the carbonate platform (Natih Fm.) integrating all presented datasets. Headings refer to the tectonic phases and captions to the structural generations I-IX (Grobe et al., 2018) and enlarged ages reflect deepest burial reached at c. 79 Ma, the onset of initial dome formation at 64 Ma (top-to-NNE shearing) and rapid exhumation active at 40 Ma. Temperatures on the right are based on RSCM and FI thermometry. Pressure at peak burial is calculated from FI measurements and independently determined temperature data to p_P= 254 ± 30 MPa and p_L= 340 MPa. The exhumation history is reconstructed from ZHe ages.

5.2.   Exhumation history

Our new thermochronology data from the central part of the Jebel Akhdar Dome suggest cooling below the reset temperature of the ZHe thermochronometer (c. 130-170 °C) between 48.7 ± 1.8 and 39.8 ± 3.0 Ma (Table 2, Figure 4). The small variation in cooling ages for the different stratigraphic levels indicates rapid passage of the entire rock suite through the ZHe partial retention zone, and consequently rapid exhumation of the Jebel Akhdar Dome. This Eocene cooling is in agreement with ZHe ages of pre-Permian strata of Hansman et al. (2017) ranging between 62 ± 3 and 39 ± 2 Ma. Apatite fission track (AFT) ages measured in the basement of the Jebel Akhdar range between 55 ± 5 Ma and 48 ± 7 Ma (4 samples, Poupeau et al., 1998) and 51 ± 8 Ma to 32 ± 4 Ma (Hansman et al., 2017). The temperature of resetting the AFT system (i.e. the depth of the base of the partial annealing zone) may vary depending on annealing kinetics. For different apatite crystals this temperature ranges between 100 and 120 °C (Carlson et al., 1999; Fitzgerald et al., 2006). Hence, these AFT ages reproduce within error with our ZHe results, despites the fact that both systems are sensitive to different temperature intervals (100-120 °C and 130-170 °C, respectively This supports the interpretation of rapid exhumation of the Jebel Akhdar at c. 55 Ma. Zircon fission track ages witness cooling of the Jebel Akhdar below c. 260 °C between 96 and 70 Ma (Saddiqi et al., 2006). This implies slow cooling thereafter (c. 100° between 70 and 55 Ma) until rapid exhumation at c. 55 Ma. Earlier exhumation would not result in required thermal maturities as exposure of the rock to highest temperatures would be too short for thermal equilibration. A reheating event in the late Miocene is not required to explain the data.

Our ZHe data from the Muti Formation and the Hawasina Nappes show a spread in ages, between 173 and 43 Ma, i.e. partly much older than the ages observed in the stratigraphically lower units in the center of the dome.

A spread in (U-Th)/He-ages is often observed, and has been attributed to radiation damage density, uneven distribution of mother isotopes in the dated crystal, broken grains, grain chemistry, among other causes (e.g. Flowers et al., 2009; Guenther et al., 2013). Several studies show that samples from sedimentary rocks are particularly prone to spread in ages (e.g. von Hagke et al., 2012; Ketcham et al., 2018; Levina et al., 2014). This is because transported grains are subject to abrasion, which influences age correction for grain geometry and may obscure presence of inclusions within the crystal. Additionally, dated grains can originate from different sources, and thus have a different chemical composition and a different pre-depositional temperature history. This may result in different reset temperatures, and consequently different grains (or grain age populations) represent different thermochronometers.

It is difficult to prove the existence of such multiple thermochronometers, as independent parameters indicative for different kinetics have not yet been established. Indeed, statistical analysis of different grain age populations requires dating of multiple grains (e.g. to be 95 % certain that a population representing 5 % of the grains is not missed 117 single grain ages need to be dated, Vermeesch (2004)). In any case, reproducing ages determined in different samples indicates the data is geologically meaningful, i.e. the observed spread is the result of partial resetting and/or different kinetics and not the result of factors independent of the time-temperature history, such as undetected inclusions or external helium implantation. We thus interpret the system as only partially reset, implying these units were not heated above the reset temperature (approximately 130-170 °C) after deposition. This interpretation is corroborated by unreset ZHe ages in the Hawasina Window (Figure 1, Csontos, pers. comm.). The top of the Natih Formation experienced temperatures above 220 °C. We suggest that this apparent contradiction may be explained by juxtaposition of the colder Muti and Hawasina units against the top of the carbonate platform during extensional top-to-NNE shearing. This implies that at least 50 °C of cooling are

associated with post obduction extension, i.e. before doming. A two-stage exhumation history of the Jebel Akhdar Dome has also been inferred from structural data (Grobe et al., 2018; Mattern and Scharf, 2018) and the stratigraphic record (Fournier et al., 2006; Mann et al., 1990). Top-to-NNE shearing is associated with tectonic thinning of the ophiolite (Grobe et al., 2018). This tectonic denudation will also result in cooling, and may explain why so little ophiolite is found in the post-obduction sediments. Additionally, ophiolitic material may have been lost to the Gulf of Oman.

5.3.   Pressure evolution

Evolution of pore pressures was modelled (Figures S7 and S8) assuming a seal on top of the Natih Fm. (k_{Muti}=10^{-23} m²). Porosity was lost during Muti deposition in the moving forebulge (top seal) and related burial, the emplacement of the Hawasina Nappes and the ophiolite, which induced compaction and a remaining very low porosity of c. 1 %. Hydrostatic pressure increased with burial under the moving forebulge at 88 Ma to 40 MPa, after Muti deposition to 60 MPa and after ophiolite emplacement to 120 MPa. Calculated pore pressure rise above hydrostatic pressure in response to Hawasina Nappe and ophiolite emplacement.

Formation of tensile fractures, as inferred from bedding confined, Mode-I veins in the Natih Fm. (Arndt et al., 2014; Grobe et al., 2018; Holland et al., 2009a; Virgo, 2015), require internal fluid pressures (P_f) exceeding the sum of the stress acting normal on the fracture surface (σ_3) and the tensile stress of the rock (T): $P_f > \sigma_3 + T$, and a differential stress ($\sigma_1 - \sigma_3$) below 4T (Secor, 1965). Host-rock buffered vein isotope compositions indicate that the veins were formed by local fluids (Arndt et al., 2014) and, hence, require local overpressure cells.

Sensitivity analyses of reduced permeabilities of Muti, Natih and Nahr Umr formations show that overpressure generation, necessary for rock fracturing, requires a very good top seal and also a reduced horizontal permeability of the Natih Fm. of 10^{-23} m² (Figure S7 and S8). A top seal on its own is not sufficient for overpressures initiating rock failure. This case results in pore pressures up to 300 MPa within the top Natih and localized overpressures of 195 MPa in front of the obducting ophiolite.

All results indicate that without low horizontal permeabilities of the Natih Fm. $\leq 10^{-23}$ m² overpressure cells required for vein formation cannot be generated. The reduced permeabilities in the Natih Fm. are necessary to prevent an early, tectonically-driven horizontal pressure release.

5.4.   Fluid migration

Numerical basin modeling shows that rapid burial of sedimentary rocks below the ophiolite (88-80 Ma) caused under-compaction, i.e. a porosity too high with respect to burial depth, and consequent pore pressure increase. Two example model results of fluid migration in front of the obducting ophiolite are shown in the electronic supplement Figure S9. If low permeabilities are assigned to the non-source-rock members of the Natih Fm., migration will mainly take place within the source rocks and at layer interfaces within the Natih Fm. If the complete Natih Fm. has low permeabilities, fluids will leave the source rock vertically first, before lateral migration localizes along layer boundaries. The pressure gradient between overpressures below the allochthonous nappes and the less deeply buried southern foreland initiates tectonically-driven fluid migration in front of the obducting nappes, an idea that was first introduced by Oliver (1986). Solid bitumen accumulations in black stained calcite veins are in agreement with this interpretation (Fink et al., 2015).

719 Dome formation of the Jebel Akhdar anticline around 55 Ma initiated layer tilting and consequent southward
720 migration of the generated hydrocarbons as observed by secondary low reflective solid bitumen generations in
721 Natih veins and host rocks at the southern flank of the Oman Mountains (Fink et al., 2015; Grobe et al., 2016).

6. Conclusions

723 This study provides insights into the temperature evolution during obduction, prior to subsequent orogenesis.
724 Arabia's passive continental margin was buried to at least 4 km at times of foredeep migration and afterwards
725 under 8-10 km of Semail Ophiolite and 2 km of sedimentary Hawasina Nappes. Deepest burial under the ophiolite
726 resulted in peak temperatures of up to 300 °C (Shu'aiba Fm.) with sub-lithostatic pore pressures. Ophiolite
727 obduction and overpressure cells expelled fluids towards the foreland, through matrix and fracture porosity.
728 ZHe data show cooling associated with forebulge migration, as well as with exhumation of the Jebel Akhdar Dome.
729 Exhumation of the Jebel Akhdar Dome took place in two stages. A first stage is associated with top-to-NNE
730 shearing, which is responsible for at least 50 °C of cooling, as witnessed by juxtaposition of units including
731 partially reset ZHe ages against units that experienced more than 220 °C. ZHe data show the second exhumation
732 phase, associated with doming of the Jebel Akhdar occurred between 49 and 39 Ma.

Author contribution

734 JLU, RL and AG initiated and planned the study. AG planned and carried out fieldwork as well as thermal maturity
735 measurements (VR, solid bitumen reflectance, Raman spectroscopy), structural interpretations and basin
736 modelling. AG, CvH, JU, ID and FW carried out fieldwork and structural interpretations. FW and ID conducted
737 the thermochronological measurements with help of CvH. PM and AG performed fluid inclusion thermometry.
738 AG and CvH prepared the manuscript with contributions from all co-authors.

Acknowledgements

740 We acknowledge the highly-appreciated help of Donka Macherey (sample preparation, RWTH Aachen), the team
741 of the KU Leuven (fluid inclusion measurements) and Keno Lünsdorf (Raman spectroscopy, Georg-August-
742 University, Göttingen). Sample crushing was realized by the team of SELFRAG, Switzerland. Wiekert Visser and
743 Victoria Sachse are thanked for fruitful discussions; Gösta Hoffmann and Wilfried Bauer of GUtech are thanked
744 for helping with field logistics. We are grateful for comments of Edwin Gnos, Andreas Scharf, Wolf-Christian
745 Dullo and Mark Handy on earlier versions of this manuscript and the reviews of Massimiliano Zattin, Luca Aldega,
746 Bruce Levell and Federico Rossetti.

References

748 Agard, P., Omrani, J., Jolivet, L. and Mouthereau, F.: Convergence history across Zagros (Iran): constraints from
749 collisional and earlier deformation, Int. J. Earth Sci., 94(3), 401–419, doi:10.1007/s00531-005-0481-4, 2005.
750 Al-Lazki, A. I., Seber, D., Sandvol, E. and Barazangi, M.: A crustal transect across the Oman Mountains on the
751 eastern margin of Arabia, GeoArabia, 7(1), 47–78, 2002.
752 Al-Wardi, M. and Butler, R. W. H.: Constrictional extensional tectonics in the northern Oman mountains, its role

753 in culmination development and the exhumation of the subducted Arabian continental margin, Geol. Soc. London,

754 Spec. Publ., 272(1), 187–202, doi:10.1144/GSL.SP.2007.272.01.11, 2007.

755 Aldega, L., Carminati, E., Scharf, A., Mattern, F. and Al-Wardi, M.: Estimating original thickness and extent of

756 the Semail Ophiolite in the eastern Oman Mountains by paleothermal indicators, Mar. Pet. Geol., 84, 18–33,

757 doi:10.1016/j.marpetgeo.2017.03.024, 2017.

758 Aldega, L., Bigi, S., Carminati, E., Trippetta, F., Corrado, S. and Kavoosi, M. A.: The Zagros fold-and-thrust belt

759 in the Fars province (Iran): II. Thermal evolution, Mar. Pet. Geol., 93, 376–390,

760 doi:10.1016/J.MARPETGEO.2018.03.022, 2018.

761 Aoya, M., Kouketsu, Y., Endo, S., Shimizu, H., Mizukami, T., Nakamura, D. and Wallis, S.: Extending the

762 applicability of the Raman carbonaceous-material geothermometer using data from contact metamorphic rocks, J.

763 Metamorph. Geol., 28(9), 895–914, doi:10.1111/j.1525-1314.2010.00896.x, 2010.

764 Arndt, M., Virgo, S., Cox, S. F. and Urai, J. L.: Changes in fluid pathways in a calcite vein mesh (Natih Fm, Oman

765 Mountains): insights from stable isotopes, Geofluids, 14(4), 391–418, doi:10.1111/gfl.12083, 2014.

766 Barker, C. E. E. and Pawlewicz, M. J. J.: Calculation of vitrinite reflectance from thermal histories and peak

767 temperatures, in Vitrinite Reflectance as a Maturity Parameter, vol. 570, edited by P. Mukhopadhyay and W. Dow,

768 pp. 216–229, American Chemical Society., 1994.

769 Béchennec, F., Metour, J. L. E., Rabu, D., Villey, M. and Beurrier, M.: The Hawasina Basin: A fragment of a

770 starved passive continental margin, thrust over the Arabian Platform during obduction of the Sumail Nappe,

771 Tectonophysics, 151(1–4), 323–343, doi:10.1016/0040-1951(88)90251-X, 1988.

772 Béchennec, F., Le Metour, J., Rabu, D., Bourdillon-de-Grissac, C., de Wever, P., Beurrier, M. and Villey, M.: The

773 Hawasina Nappes: stratigraphy, palaeogeography and structural evolution of a fragment of the south-Tethyan

774 passive continental margin, Geol. Soc. London, Spec. Publ., 49(1), 213–223,

775 doi:10.1144/GSL.SP.1992.049.01.14, 1990.

776 Bernoulli, D., Weissert, H. and Blome, C. D.: Evolution of the Triassic Hawasina Basin, Central Oman Mountains,

777 Geol. Soc. London, Spec. Publ., 49(1), 189–202, doi:10.1144/GSL.SP.1992.049.01.12, 1990.

778 Beurrier, M., Bechennec, F., Rabu, D. and Hutin, G.: Geological Map of Rustaq - explanatory notes, Sultanat

779 Oman, Minist. Pet. Miner., 1986.

780 Beyssac, O., Goffé, B., Chopin, C. and Rouzaud, J. N.: Raman spectra of carbonaceous material in metasediments:

781 A new geothermometer, J. Metamorph. Geol., 20, 859–871, doi:10.1046/j.1525-1314.2002.00408.x, 2002.

782 Bodnar, R. J.: Revised equation and table for determining the freezing point depression of H2O-NaCl solutions,

783 Gechimica Cosmochim. Acta, 57, 683–684, 1993.

784 Breton, J. P., Béchennec, F., Le Métour, J., Moen-Maurel, L. and Razin, P.: Eoalpine (Cretaceous) evolution of

785 the Oman Tethyan continental margin: Insights from a structural field study in Jabal Akhdar (Oman Mountains),

786 GeoArabia, 9(2), 41–58, 2004.

787 Brown, P. E.: FLINCOR; a microcomputer program for the reduction and investigation of fluid-inclusion data,

788 Am. Mineral., 74, 1390–1393, 1989.

789 Van Buchem, F. S. P., Razin, P., Homewood, P. W., Philip, J. M., Eberli, G. P., Platel, J. P., Roger, J., Eschard,

790 R., Desaubliaux, G. M. J., Boisseau, T., Leduc, J. P., Labourdette, R. and Cantaloube, S.: High resolution sequence

791 stratigraphy of the Natih Formation (Cenomanian/Turonian) in northern Oman: distribution of source rocks and

792 reservoir facies, GeoArabia, 1(1), 65–91, 1996.

793 Van Buchem, F. S. P., Razin, P., Homewood, P. W., Oterdoom, W. H. and Philip, J.: Stratigraphic organization of

794 carbonate ramps and organic- rich intrashelf basins: Natih Formation (middle Cretaceous) of northern Oman, Am.
795 Assoc. Pet. Geol. Bull., 86(1), 21–53, doi:10.1306/61EEDA30-173E-11D7-8645000102C1865D, 2002.

796 Carlson, W. D., Donelick, R. A. and Ketcham, R. A.: Variability of apatite fission-track annealing kinetics: I.
797 Experimental results, Am. Mineral., 84(9), 1213–1223, doi:10.2138/am-1999-0901, 1999.

798 Claringbould, J. S., Hyden, B. B., Sarg, J. F. and Trudgill, B. D.: Structural evolution of a salt-cored, domed,
799 reactivated fault complex, Jebel Madar, Oman, J. Struct. Geol., 51, 118–131, doi:10.1016/j.jsg.2013.03.001, 2013.

800 Coleman, R. G.: Tectonic Setting for Ophiolite Obduction in Oman, J. Geophys. Res., 86(B4), 2497–2508, 1981.

801 Cooper, D. J. W., Ali, M. Y. and Searle, M. P.: Structure of the northern Oman Mountains from the Semail
802 Ophiolite to the Foreland Basin, Geol. Soc. London, Spec. Publ., 392, 129–153, 2014.

803 Cowan, R. J., Searle, M. P. and Waters, D. J.: Structure of the metamorphic sole to the Oman Ophiolite, Sumeini
804 Window and Wadi Tayyin: implications for ophiolite obduction processes, Geol. Soc. London, Spec. Publ., 392(1),
805 155–175, doi:10.1144/SP392.8, 2014.

806 Deville, E. and Sassi, W.: Contrasting thermal evolution of thrust systems: An analytical and modeling approach
807 in the front of the western Alps, Am. Assoc. Pet. Geol. Bull., 90(6), 887–907, doi:10.1306/01090605046, 2006.

808 Duretz, T., Agard, P., Yamato, P., Ducassou, C. C. C., Burov, E. B. and Gerya, T. V.: Thermo-mechanical
809 modeling of the obduction process based on the Oman Ophiolite case, Gondwana Res.,
810 doi:10.1016/j.gr.2015.02.002, 2015.

811 Ferreiro Mählmann, R.: Correlation of very low grade data to calibrate a thermal maturity model in a nappe tectonic
812 setting, a case study from the Alps, Tectonophysics, 334, 1–33, 2001.

813 Filbrandt, J. B., Al-Dhahab, S., Al-Habsy, A., Harris, K., Keating, J., Al-mahruqi, S., Ozkaya, S. I., Richard, P. D.
814 and Robertson, T.: Kinematic interpretation and structural evolution of North Oman, Block 6, since the Late
815 Cretaceous and implications for timing of hydrocarbon migration into Cretaceous reservoirs, GeoArabia, 11(1),
816 97–115, 2006.

817 Fink, R., Virgo, S., Arndt, M., Visser, W., Littke, R. and Urai, J. L. L.: Solid bitumen in calcite veins from the
818 Natih Formation in the Oman Mountains: multiple phases of petroleum migration in a changing stress field, Int. J.
819 Coal Geol., 157, 39–51, doi:10.1016/j.coal.2015.07.012, 2015.

820 Fitzgerald, P. G., Baldwin, S. L., Webb, L. E. and O'Sullivan, P. .: He data from slowly cooled crustal terranes
821 and the interpretation of intra-sample variations of single crystal apatite ages from vertical profiles., Chem. Geol.,
822 225, 91–120, 2006.

823 Flowers, R. M., Ketcham, R. A., Shuster, D. L. and Farley, K. A.: Apatite (U–Th)/He thermochronometry using a
824 radiation damage accumulation and annealing model, Geochim. Cosmochim. Acta, 73(8), 2347–2365,
825 doi:10.1016/J.GCA.2009.01.015, 2009.

826 Forbes, G. A., Jansen, H. S. M. and Schreurs, J.: Lexicon of Oman - Subsurface Stratigraphy - Reference Guide
827 to the Stratigraphy of Oman's Hydrocarbon Basins, GeoArabia Spec. Publ. 5, 2010.

828 Fournier, M., Lepvrier, C., Razin, P. and Jolivet, L.: Late Cretaceous to Paleogene post-obduction extension and
829 subsequent Neogene compression in the Oman Mountains, GeoArabia, 11(4), 17–40, 2006.

830 Glennie, K. W., Boeuf, M. G. A., Clarke, M. W. H., Moody-Stuart, M., Pilaar, W. F. H. and Reinhardt, B. M.:
831 Late Cretaceous Nappes in Oman Mountains and Their Geologic Evolution : Reply, Am. Assoc. Pet. Geol. Bull.,
832 57(1), 5–27, 1973.

833 Glennie, K. W., Boeuf, M. G. A., Hughes Clarke, M. W., Moody-Stuart, M., Pilaar, W. F. H. and Reinhardt, B.
834 M.: Geology of the Oman Mountains, Verh. van het K. Ned. Geol. Mijnbouwkd. Genoot., 31, 432, 1974.

835 Gnos, E. and Peters, T.: K-Ar ages of the metamorphic sole of the Semail Ophiolite: implications for ophiolite
836 cooling history, Contrib. to Mineral. Petrol., 113, 325–332, 1993.

837 Goldstein, R. H.: Fluid inclusions in sedimentary and diagenetic systems, Lithos, 55(1–4), 159–193,
838 doi:10.1016/S0024-4937(00)00044-X, 2001.

839 Gomez-Rivas, E., Bons, P. D., Koehn, D., Urai, J. L., Arndt, M., Virgo, S., Laurich, B., Zeeb, C., Stark, L. and
840 Blum, P.: The Jabal Akhdar Dome in the Oman mountains: Evolution of a dynamic fracture system, Am. J. Sci.,
841 314(7), 1104–1139, doi:10.2475/07.2014.02, 2014.

842 Grelaud, C., Razin, P., Homewood, P. W. and Schwab, a. M.: Development of Incisions on a Periodically
843 Emergent Carbonate Platform (Natih Formation, Late Cretaceous, Oman), J. Sediment. Res., 76(4), 647–669,
844 doi:10.2110/jsr.2006.058, 2006.

845 Grobe, A., Littke, R., Urai, J. L. J. L. L., Lünsdorf, N. K. K., Littke, R. and Lünsdorf, N. K. K.: Hydrocarbon
846 generation and migration under a large overthrust: The carbonate platform under the Semail Ophiolite, Jebel
847 Akhdar, Oman, Int. J. Coal Geol., 168, 1–17, doi:10.1016/j.coal.2016.02.007, 2016.

848 Grobe, A., Virgo, S., von Hagke, C., Urai, J. L. L. and Littke, R.: Multiphase Structural Evolution of a Continental
849 Margin During Obduction Orogeny: Insights From the Jebel Akhdar Dome, Oman Mountains, Tectonics, 37(3),
850 888–913, doi:10.1002/2016TC004442, 2018.

851 Guenther, W. R., Reiners, P. W., Ketcham, R. A., Nasdala, L. and Giester, G.: American Journal of Science, Am.
852 J. Sci., 313(March), 145–198, doi:10.2475/03.2013.01, 2013.

853 Habsi, N. Al, Shukaili, M. Al, Tooqi, S. Al, Ehrenberg, S. N. and Bernecker, M.: Lithofacies, diagenesis and
854 reservoir quality of Upper Shu'aiba reservoirs in northwestern Oman, GeoArabia, 19(4), 145–182, 2014.

855 Hacker, B. R. and Mosenfelder, J. L.: Metamorphism and deformation along the emplacement thrust of the Samail
856 ophiolite, Oman, Earth Planet. Sci. Lett., 144(3–4), 435–451, doi:10.1016/S0012-821X(96)00186-0, 1996.

857 Hacker, B. R., Mosenfelder, J. L. and Gnos, E.: Rapid emplacement of the Oman ophiolite: Thermal and
858 geochronologic constraints, Tectonics, 15(6), 1230–1247, 1996.

859 von Hagke, C., Cederbom, C. E., Oncken, O., Stöckli, D. F., Rahn, M. K. and Schlunegger, F.: Linking the northern
860 Alps with their foreland: The latest exhumation history resolved by low-temperature thermochronology, Tectonics,
861 31(5), n/a-n/a, doi:10.1029/2011TC003078, 2012.

862 Hanna, S. S.: The Alpine deformation of the Central Oman Mountains, Geol. Soc. London, Spec. Publ., 49(1),
863 341–359, doi:10.1144/GSL.SP.1992.049.01.21, 1990.

864 Hansman, R. J., Ring, U., Thomson, S. N. and Brok, B. Den: Late Eocene uplift of the Al Hajar Mountains, Oman,
865 supported by stratigraphy and low-temperature thermochronology, Tectonics, doi:10.1002/2017TC004672, 2017.

866 Hansman, R. J., Albert, R., Gerdes, A. and Ring, U.: Absolute ages of multiple generations of brittle structures by
867 U-Pb dating of calcite, Geology, doi:10.1130/G39822.1, 2018.

868 Hassanzadeh, J. and Wernicke, B. P.: The Neotethyan Sanandaj-Sirjan zone of Iran as an archetype for passive
869 margin-arc transitions, Tectonics, 25(3), 586–621, doi:10.1002/2015TC003926, 2016.

870 Hilgers, C., Kirschner, D. L., Breton, J. P. P. and Urai, J. L.: Fracture sealing and fluid overpressures in limestones
871 of the Jabal Akhdar dome, Oman mountains, Geofluids, 6(2), 168–184, doi:10.1111/j.1468-8123.2006.00141.x,
872 2006.

873 Hillier, S., Mátyás, J., Matter, A. and Vasseur, G.: Illite/smectite diagenesis and its variable correlation with
874 vitrinite reflectance in the Pannonian Basin, Clays Clay Miner., 43(2), 174–183,
875 doi:10.1346/CCMN.1995.0430204, 1995.

876 Holland, M., Urai, J. L., Muchez, P. and Willemse, E. J. M.: Evolution of fractures in a highly dynamic thermal,
877 hydraulic, and mechanical system - (I) Field observations in Mesozoic Carbonates, Jabal Shams, Oman Mountains,
878 GeoArabia, 14(1), 57–110, 2009a.

879 Holland, M., Saxena, N. and Urai, J. L.: Evolution of fractures in a highly dynamic thermal, hydraulic, and
880 mechanical system - (II) Remote sensing fracture analysis, Jabal Shams, Oman mountains, GeoArabia, 14(3), 163–
881 194, 2009b.

882 Homewood, P., Razin, P., Grélaud, C., Droste, H., Vahrenkamp, V., Mettraux, M. and Mattner, J.: Outcrop
883 sedimentology of the Natih Formation, northern Oman: A field guide to selected outcrops in the Adam Foothills
884 and Al Jabal al Akhdar areas, GeoArabia, 13(3), 39–120, 2008.

885 Immenhauser, A. and Scott, R. W.: An estimate of Albian sea-level amplitudes and its implication for the duration
886 of stratigraphic hiatuses, Sediment. Geol., 152(1–2), 19–28, doi:10.1016/S0037-0738(02)00260-9, 2002.

887 Immenhauser, A., Schlager, W., Burns, S. J., Scott, R. W., Geel, T., Lehmann, J., van der Gaast, S. and Bolder-
888 Schrijver, L. J. A. J. a.: Late Aptian to late Albian sea-level fluctuations constrained by geochemical and biological
889 evidence (Nahr Umr Formation, Oman), J. Sediment. Res., 69(2), 434–446, doi:10.2110/jsr.69.434, 1999.

890 Jacobs, J., Thomas, R. J., Ksienzyk, A. K. and Dunkl, I. I.: Tracking the Oman Ophiolite to the surface - New
891 fission track and (U-Th)/He data from the Aswad and Khor Fakkan Blocks, United Arab Emirates, Tectonophysics,
892 644, 68–80, doi:10.1016/j.tecto.2014.12.018, 2015.

893 Jirman, P., Geršlová, E., Kalvoda, J. and Melichar, R.: 2d basin modelling in the eastern variscan fold belt (Czech
894 Republic): influence of thrusting on patterns of thermal maturation, J. Pet. Geol., 41(2), 175–188,
895 doi:10.1111/jpg.12699, 2018.

896 De Keijzer, M., Hillgartner, H., Al Dhahab, S. and Rawnsley, K.: A surface-subsurface study of reservoir-scale
897 fracture heterogeneities in Cretaceous carbonates, North Oman, Geol. Soc. London, Spec. Publ., 270(1), 227–244,
898 doi:10.1144/GSL.SP.2007.270.01.15, 2007.

899 Ketcham, R. A.: Forward and Inverse Modeling of Low-Temperature Thermochronometry Data, Rev. Mineral.
900 Geochemistry, 58, 275–314, doi:10.2138/rmg.2005.58.11, 2005.

901 Ketcham, R. A., Mora, A. and Parra, M.: Deciphering exhumation and burial history with multi-sample down-well
902 thermochronometric inverse modelling, Basin Res., 30, 48–64, doi:10.1111/bre.12207, 2018.

903 Koehrer, B., Zeller, M., Aigner, T., Poeppelreiter, M., Milroy, P., Forke, H. and Al-Kindi, S.: Facies and
904 stratigraphic framework of a Khuff outcrop equivalent: Saiq and Mahil formations, Al Jabal al-Akhdar, Sultanate
905 of Oman, GeoArabia, 15(2), 91–156, 2010.

906 Koehrer, B., Aigner, T. and Poppelreiter, M.: Field-scale geometries of Upper Khuff reservoir geobodies in an
907 outcrop analogue (Oman Mountains, Sultanate of Oman), Pet. Geosci., 17(1), 3–16, doi:10.1144/1354-079310-
908 009, 2011.

909 Kouketsu, Y., Mizukami, T., Mori, H., Endo, S., Aoya, M., Hara, H., Nakamura, D. and Wallis, S.: A new approach
910 to develop the Raman carbonaceous material geothermometer for low-grade metamorphism using peak width, Isl.
911 Arc, 23, 33–50, doi:10.1111/iar.12057, 2014.

912 Levina, M., Horton, B. K., Fuentes, F. and Stockli, D. F.: Cenozoic sedimentation and exhumation of the foreland
913 basin system preserved in the Precordillera thrust belt (31-32°S), southern central Andes, Argentina, Tectonics,
914 33(9), 1659–1680, doi:10.1002/2013TC003424, 2014.

915 Lippard, S. J., Smewing, J. D., Rothery, D. a. and Browning, P.: The geology of the Dibba zone, northern Oman
916 mountains - a preliminary study, J. Geol. Soc. London., 139(1), 59–66, doi:10.1144/gsjgs.139.1.0059, 1982.

917 Loosveld, R. J. H., Bell, A. and Terken, J. J. M.: The Tectonic Evolution of Interior Oman, GeoArabia, 1(1), 28–

918 51 [online] Available from: http://search.ebscohost.com/login.aspx?direct=true&db=geh&AN=1998-

919 061521&site=ehost-live&scope=cite, 1996.

920 Lünsdorf, N. K.: Raman spectroscopy of dispersed vitrinite - methodical aspects and correlation with reflectance,

921 Int. J. Coal Geol., 153(1), 75–86, doi:10.1016/j.coal.2015.11.010, 2016.

922 Lünsdorf, N. K., Dunkl, I., Schmidt, B. C., Rantitsch, G. and von Eynatten, H.: The thermal history of the Steinach

923 Nappe (eastern Alps) during extension along the Brenner Normal Fault system indicated by organic maturation

924 and zircon (U-Th)/ He thermochronology, Austrian J. Earth Sci., 105(3), 17–25, 2012.

925 Lünsdorf, N. K., Dunkl, I., Schmidt, B. C., Rantitsch, G. and von Eynatten, H.: Towards a Higher Comparability

926 of Geothermometric Data Obtained by Raman Spectroscopy of Carbonaceous Material. Part 2: A Revised

927 Geothermometer, Geostand. Geoanalytical Res., 41(4), 593–612, doi:10.1111/ggr.12178, 2017.

928 Mair, D., Lechmann, A., Herwegh, M., Nibourel, L. and Schlunegger, F.: Linking Alpine deformation in the Aar

929 Massif basement and its cover units – the case of the Jungfrau–Eiger mountains (Central Alps, Switzerland), Solid

930 Earth, 9(5), 1099–1122, doi:10.5194/se-9-1099-2018, 2018.

931 Mann, a., Hanna, S. S. and Nolan, S. C.: The post-Campanian tectonic evolution of the Central Oman Mountains:

932 Tertiary extension of the Eastern Arabian Margin, Geol. Tectonics Oman Reg., 49(1), 549–563,

933 doi:10.1144/gsl.sp.1992.049.01.33, 1990.

934 Mashhadi, Z. S., Rabbani, A. R. and Kamali, M. R.: Geochemical characteristics and hydrocarbon generation

935 modeling of the Kazhdumi (Early Cretaceous), Gurpi (Late Cretaceous) and Pabdeh (Paleogene) formations,

936 Iranian sector of the Persian Gulf, Mar. Pet. Geol., 66, 978–997, doi:10.1016/J.MARPETGEO.2015.08.008, 2015.

937 Mattern, F. and Scharf, A.: Postobductional extension along and within the Frontal Range of the Eastern Oman

938 Mountains, J. Asian Earth Sci., 154, doi:10.1016/j.jseaes.2017.12.031, 2018.

939 Le Metour, J., Rabu, D., Tegyey, M., Bechennec, F., Beurrier, M. and Villey, M.: Subduction and obduction: two

940 stages in the EoAlpine tectonometamorphic evolution of the Oman Mountains, Geol. Soc. London, Spec. Publ.,

941 49(1), 327–339, doi:10.1144/GSL.SP.1992.049.01.20, 1990.

942 Mouthereau, F.: Timing of uplift in the Zagros belt/Iranian plateau and accommodation of late Cenozoic Arabia -

943 Eurasia convergence, Geol. Mag., 148(5–6), 726–738, doi:10.1017/S0016756811000306, 2011.

944 Mozafari, M., Swennen, R., Balsamo, F., Clemenzi, L., Storti, F., El Desouky, H., Vanhaecke, F., Tueckmantel,

945 C., Solum, J. and Taberner, C.: Paleofluid Evolution In Fault-Damage Zones: Evidence From Fault-Fold

946 Interaction Events In the Jabal Qusaybah Anticline (Adam Foothills, North Oman), J. Sediment. Res., 85(12),

947 1525–1551, doi:10.2110/jsr.2015.95, 2015.

948 Muchez, P., Marshall, J. D., Touret, J. L. R. and Viaene, W. a.: Origin and migration of palaeofluids in the Upper

949 Visean of the Campine Basin, northern Belgium, Sedimentology, 41(1), 133–145, doi:10.1111/j.1365-

950 3091.1994.tb01395.x, 1994.

951 Neumaier, M.: Structural Restoration and Basin and Petroleum Systems Modeling: Case Studies from the Monagas

952 Fold and Thrust Belt, Venezuela and the Moroccan Atlantic Margin, Dissertation, RWTH Aachen University.,

953 2015.

954 Nibourel, L., Berger, A., Egli, D., Luensdorf, N. K. and Herwegh, M.: Large vertical displacements of a crystalline

955 massif recorded by Raman thermometry, Geology, 46(10), 879–882, doi:10.1130/G45121.1, 2018.

956 Nicolas, A. and Boudier, F. F.: Structural contribution from the Oman ophiolite to processes of crustal accretion

957 at the East Pacific Rise, Terra Nov., 27(2), 77–96, doi:10.1111/ter.12137, 2015.

958 Nolan, S. C., Skelton, P. W., Clissold, B. P. and Smewing, J. D.: Maastrichtian to early Tertiary stratigraphy and
959 palaeogeography of the Central and Northern Oman Mountains, Geol. Soc. London, Spec. Publ., 49(1), 495–519,
960 doi:10.1144/gsl.sp.1992.049.01.31, 1990.

961 Nöth, S., Karg, H. and Littke, R.: Reconstruction of Late Paleozoic heat flows and burial histories at the
962 Rhenohercynian-Subvariscan boundary, Germany, Int. J. Earth Sci., 90(2), 234–256, doi:10.1007/s005310000114,
963 2001.

964 Oliver, J.: Fluids expelled tectonically from orogenic belts: Their role in hydrocarbon migration and other geologic
965 phenomena, Geology, 14(February), 99–102, 1986.

966 Oxburgh, E. R. and Turcotte, D. L.: Thermal gradients and regional metamorphism in overthrust terrains with
967 special reference to the Eastern Alps, Schweizerische Mineral. und Petrogr. Mitteilungen, 54(2/3), 642–662, 1974.

968 Philip, J., Borgomano, J. and Al-Maskiry, S.: Cenomanian-Early Turonian carbonate platform of Northern Oman:
969 stratigraphy and palaeo-environments, Palaeogeogr. Palaeoclimatol. Palaeoecol., 119, 77–92, 1995.

970 Pöppelreiter, M. C., Schneider, C. J., Obermaier, M., Forke, H. C., Koehrer, B. and Aigner, T.: Seal turns into
971 reservoir: Sudair equivalents in outcrops, A1 Jabal al-Akhdar, Sultanate of Oman, GeoArabia, 16(1), 69–108,
972 2011.

973 Poupeau, G., Saddiqi, O., Michard, A., Goffé, B. and Oberhänsli, R.: Late thermal evolution of the Oman
974 Mountains subophiolitic windows: Apatite fission-track thermochronology, Geology, 26(12), 1139–1142, 1998.

975 Pratt, R., Smewing, D., Swansea, S. A., Pratt, B. R. and Smewing, J. D.: Jurassic and Early Cretaceous platform
976 margin configuration and evolution, central Oman Mountains, Geol. Soc. London, Spec. Publ., 49(1), 69–88,
977 doi:10.1144/GSL.SP.1992.049.01.06, 1990.

978 Rabu, D., Le Metour, J., Bechennec, F., Beurrier, M., Villey, M. and Bourdillon-Jeudy de Grissac, C.: Sedimentary
979 aspects of the Eo-Alpine cycle on the northeast edge of the Arabian Platform (Oman Mountains), Geol. Soc.
980 London, Spec. Publ., 49(1), 49–68, doi:10.1144/GSL.SP.1992.049.01.05, 1990.

981 Rantitsch, G. and Rainer, T.: Thermal modeling of Carboniferous to Triassic sediments of the Karawanken Range
982 (Southern Alps) as a tool for paleogeographic reconstructions in the Alpine-Dinaridic-Pannonian realm, Int. J.
983 Earth Sci., 92(2), 195–209, doi:10.1007/s00531-003-0312-4, 2003.

984 Reiners, P. W.: Zircon (U-Th)/He Thermochronometry, Rev. Mineral. Geochemistry, 58(1936), 151–179,
985 doi:10.2138/rmg.2005.58.6, 2005.

986 Reutter, K.-J., Teichmüller, M. and Teichmüller, R.: The Coalification Pattern in the Northern Apennines and its
987 Palaeogeothermic and Tectonic Significance, Geol. RundschauGeologische Rundschau, 72(3), 861–894, 1988.

988 Rioux, M., Bowring, S., Kelemen, P., Gordon, S., Miller, R. and Dudás, F.: Tectonic development of the Samail
989 ophiolite: High-precision U-Pb zircon geochronology and Sm-Nd isotopic constraints on crustal growth and
990 emplacement, J. Geophys. Res. Solid Earth, 118(5), 2085–2101, doi:10.1002/jgrb.50139, 2013.

991 Rioux, M., Garber, J., Bauer, A., Bowring, S., Searle, M., Kelemen, P. and Hacker, B.: Synchronous formation of
992 the metamorphic sole and igneous crust of the Semail ophiolite: New constraints on the tectonic evolution during
993 ophiolite formation from high-precision U–Pb zircon geochronology, Earth Planet. Sci. Lett., 451, 185–195,
994 doi:10.1016/j.epsl.2016.06.051, 2016.

995 Robertson, A.: The transition from a passive margin to an Upper Cretaceous foreland basin related to ophiolite
996 emplacement in the Oman Mountains, Geol. Soc. Am. Bull., 99, 633–653, doi:10.1130/0016-7606(1987)99<633,
997 1987.

998 Rolandone, F., Lucazeau, F., Leroy, S., Mareschal, J.-C., Jorand, R., Goutorbe, B. and Bouquerel, H.: New heat

999 flow measurements in Oman and the thermal state of the Arabian Shield and Platform, Tectonophysics, 589, 77–
1000 89, doi:10.1016/j.tecto.2012.12.034, 2013.

1001 Roure, F., Andriessen, P., Callot, J. P., Faure, J. L., Ferket, H., Gonzales, E., Guilhaumou, N., Lacombe, O.,
1002 Malandain, J., Sassi, W., Schneider, F., Swennen, R., Vilasi, N., Box, P. O., Gonzales, E., Guilhaumou, N.,
1003 Lacombe, O., Malandain, J., Sassi, W., Schneider, F., Swennen, R. and Vilasi, N.: The use of palaeo-thermo-
1004 barometers and coupled thermal, fluid flow and pore-fluid pressure modelling for hydrocarbon and reservoir
1005 prediction in fold and thrust belts, Geol. Soc. London, Spec. Publ., 348(1), 87–114, doi:10.1144/SP348.6, 2010.

1006 Saddiqi, O., Michard, A. N., Goffe, B. R., Poupeau, G. É. and Oberhänsli, R. O.: Fission-track thermochronology
1007 of the Oman Mountains continental windows, and current problems of tectonic interpretation, Bull. la Soc. Geol.
1008 Fr., 177(3), 127–143, doi:10.2113/gssgfbull.177.3.127, 2006.

1009 Schito, A., Corrado, S., Trolese, M., Aldega, L., Caricchi, C., Cirilli, S., Grigo, D., Guedes, A., Romano, C., Spina,
1010 A. and Valentim, B.: Assessment of thermal evolution of Paleozoic successions of the Holy Cross Mountains
1011 (Poland), Mar. Pet. Geol., 80, 112–132, doi:10.1016/J.MARPETGEO.2016.11.016, 2017.

1012 Schito, A., Andreucci, B., Aldega, L., Corrado, S., Di Paolo, L., Zattin, M., Szaniawski, R., Jankowski, L. and
1013 Mazzoli, S.: Burial and exhumation of the western border of the Ukrainian Shield (Podolia): a multi-disciplinary
1014 approach, Basin Res., 30, 532–549, doi:10.1111/bre.12235, 2018.

1015 Scott, R. W.: Chronostratigraphy of the Cretaceous carbonate shelf, southeastern Arabia, Geol. Soc. London, Spec.
1016 Publ., 49(1), 89–108, doi:10.1144/GSL.SP.1992.049.01.07, 1990.

1017 Searle, M. P.: Sequence of thrusting and origin of culminations in the northern and central Oman Mountains, J.
1018 Struct. Geol., 7(2), 129–143, doi:10.1016/0191-8141(85)90127-0, 1985.

1019 Searle, M. P. and Cox, J. O. N.: Subduction zone metamorphism during formation and emplacement of the Semail
1020 ophiolite in the Oman Mountains, Geol. Mag., 139(03), 241–255, doi:10.1017/S0016756802006532, 2002.

1021 Searle, M. P., Warren, C. J., Waters, D. J. and Parrish, R. R.: Subduction zone polarity in the Oman Mountains:
1022 implications for ophiolite emplacement, Geol. Soc. London, Spec. Publ., 218(1), 467–480,
1023 doi:10.1144/GSL.SP.2003.218.01.24, 2003.

1024 Searle, M. P., Warren, C. J. J., Waters, D. . J. and Parrish, R. . R.: Structural evolution, metamorphism and
1025 restoration of the Arabian continental margin, Saih Hatat region, Oman Mountains, J. Struct. Geol., 26(3), 451–
1026 473, doi:10.1016/j.jsg.2003.08.005, 2004.

1027 Searle, M. P. M. P.: Structural geometry, style and timing of deformation in the Hawasina Window, Al Jabal al
1028 Akhdar and Saih Hatat culminations, Oman Mountains, GeoArabia, 12(2), 99–130, 2007.

1029 Secor, D. T. jr.: Role of fluid pressure in jointing, Am. J. Sci., 263(October), 633–646, 1965.

1030 Stenhouse, P.: Reactive Transport and Fluid Pathways in Fracture-Controlled Flow Systems, (Doctoral
1031 Dissertation)., Australian National University., 2014.

1032 Sweeney, J. J. and Burnham, A. K.: Evaluation of a Simple Model of Vitrinite Reflectance Based on Chemical
1033 Kinetics, Am. Assoc. Pet. Geol. Bull., 74(10), 1559–1570, 1990.

1034 Teichmüller, R. and Teichmüller, M.: Relations between coalification and palaeogeothermics in Variscan and
1035 Alpidic foredeeps of western Europe, Lect. Notes Earth Sci., 5, 1986.

1036 Terken, J. M. J.: The Natih petroleum system of north Oman, GeoArabia, 4(2), 157–180, 1999.

1037 Terken, J. M. J., Frewin, N. L., Indrelid, S. L. and Indrelin, S. L.: Petroleum systems of Oman: Charge timing and
1038 risks, Am. Assoc. Pet. Geol. Bull., 85(10), 1817–1845, 2001.

1039 Vahrenkamp, V. C.: Chemostratigraphy of the Lower Cretaceous Shu'aiba Formation: A delta-13C reference

1040   profile for the Aptian Stage from the southern Neo-Tethys Ocean, GeoArabia, 1, 107–137, 2010.

1041   Velde, B. and Lanson, B.: Comparison of I/S transformation and maturity of organic matter at elevated

1042   temperatures, Clays Clay Miner., 41(2), 178–183, 1993.

1043   Vermeesch, P.: How many grains are needed for a provenance study?, Earth Planet. Sci. Lett., 224(3–4), 441–451,

1044   doi:10.1016/J.EPSL.2004.05.037, 2004.

1045   Virgo, S.: Aspects of crack-seal vein system evolution. (Doctoral Dissertation). Retrieved from http://nbn-

1046   resolving.de/urn/resolver.pl?urn=urn:nbn:de:hbz:82-opus-33858., RWTH Aachen University., 2015.

1047   Virgo, S. and Arndt, M.: Evolution of a crack-seal calcite vein network in limestone: a high resolution structural,

1048   microstructural and geochemical study from the Jebel Akhdar high pressure cell, Oman Mountains, (Diploma

1049   Thesis)., RWTH Aachen [online] Available from: http://darwin.bth.rwth-aachen.de/opus3/volltexte/2010/3385/,

1050   2010.

1051   Virgo, S., Arndt, M., Sobisch, Z. Z. and Urai, J. L.: Development of fault and vein networks in a carbonate

1052   sequence near Hayl al-Shaz, Oman Mountains, GeoArabia, 18(2), 99–136 [online] Available from:

1053   http://www.gulfpetrolink.net/publication/vol18.php, 2013a.

1054   Virgo, S., Abe, S. and Urai, J. L.: Extension fracture propagation in rocks with veins: Insight into the crack-seal

1055   process using Discrete Element Method modeling, J. Geophys. Res. Solid Earth, 118(10), 5236–5251,

1056   doi:10.1002/2013JB010540, 2013b.

1057   Visser, W.: Burial and thermal history of Proterozoic source rocks in Oman, Precambrian Res., 54(1), 15–36,

1058   doi:10.1016/0301-9268(91)90066-J, 1991.

1059   Warburton, J., Burnhill, T. J., Graham, R. H. and Isaac, K. P.: The evolution of the Oman Mountains Foreland

1060   Basin, Geol. Soc. London, Spec. Publ., 49(1), 419–427, doi:10.1144/GSL.SP.1992.049.01.26, 1990.

1061   Warren, C. J., Parrish, R. R., Searle, M. P. and Waters, D. J.: Dating the subduction of the Arabian continental

1062   margin beneath the Semail ophiolite, Oman, Geology, 31(10), 889, doi:10.1130/G19666.1, 2003.

1063   Warren, C. J., Parrish, R. R., Waters, D. J. and Searle, M. P.: Dating the geologic history of Oman's Semail

1064   ophiolite: insights from U-Pb geochronology, Contrib. to Mineral. Petrol., 150(4), 403–422, doi:10.1007/s00410-

1065   005-0028-5, 2005.

1066   Wygrala, B. P.: Integrated study on an oil field in the southern po basin, northern italy, Berichte der

1067   Kernforschungsanlage Jülich, 2313(October), 217, 1989.

1068